Cellular Physiology and Biochemistry

Cell Physiol Biochem 2016;38:1267-1287
DOI: 10.1159/000443074
Published online: March 24, 2016
Accepted: February 02, 2016

1421-9778/16/0384-1267$39.50/0
www.karger.com/cpb

Original Paper

Changes in the MicroRNA Profile of the Mandible of Ovariectomized Mice

LingYu Hao Jia Li YaWen Tian JunHua Wu

Department of Prosthodontics, School & Hospital of Stomatology, Tongji University, Shanghai Engineering Research Center of Tooth Restoration and Regeneration, Shanghai China

Key Words
MicroRNA • Mandible • Ovariectomy • MiRNA expression profile

Abstract
Background/Aims: In postmenopausal women, a decrease in bone mineral density (BMD) at the hip and spine is associated with an increased risk of tooth loss, possibly caused by the loss of the alveolar bone. The present study explored the effect of the ovariectomy (OVX) of mice on the miRNA expression profile of their bones. ***Methods:*** Micro-CT and histological analysis were performed on mice following OVX or sham-operation using the right mandibles. The left mandibles were used for microarray and quantitative RT-PCR to explore the change in their miRNA expression profile. The differentially expressed miRNAs (DEmiRs) of the OVX and sham-operated mice were analyzed by constructing the miRNA-mRNA-function complex network. We then also analyzed the different roles of the regulation of miRNAs in the mandible and femur by combining public data from GEO. ***Results:*** OVX could lead to a significant decrease in the BMD in the mandible. A total of 53 DEmiRs including, 18 up-regulated and 35 down-regulated miRNAs, were identified. The analysis of the miRNA-mRNA-pathway complex network suggested that miR-17-5p and miRNA-297a-5p were potential biomarkers in the development of mandibles of OVX mice. A comparison of the analysis data on the mandible and femur showed that the transforming growth factor-β signaling pathway was specifically regulated in the mandible, whereas the Wnt signaling pathway was specifically regulated in the femur. Moreover, miR-17-5p and miR-133a-3p showed different expression tendencies in the mandible and in the femur after OVX. ***Conclusion:*** This study provides an integrated function analysis of miRNA in mandibles after OVX and of miR-17-5p and miR-133a-3p as potential biomarkers. Moreover, the mechanism in mandibles may not be comparable with that in femurs with estrogen deficiency.

Introduction

Estrogen has a key role in maintaining healthy bones. Estrogen deficiency, which has a significantly negative effect on bone cell functions, such as osteocytes, osteoclasts, and osteoblasts, may result in bone disease-postmenopausal osteoporosis [1]. Postmenopausal

Junhua Wu

Department of Prosthodontics, School & Hospital of Stomatology, Tongji University, No. 399, Yanchang Middle Road, Shanghai 200072, (China)
Tel. +8602165982200, E-Mail junhua-wu@hotmail.com.com

osteoporosis is characterized by the severe loss of bone mass in the vertebrae and long bones. Furthermore, the structure of the mandible and alveolar bone are also affected by estrogen deficiency. Some studies have reported a positive correlation between osteoporosis and mandible conditions, such as tooth loss [2, 3], low bone mineral density (BMD) in the mandible [4-6], and periodontal status [7, 8]. Moreover, according to the steadily declining trend of BMD of long bones and mandible induced by estrogen deficiency, systemic osteoporosis can be predicted with BMD in the mandible [9].

The reliability of ovariectomized (OVX) animals as mandibular osteoporotic models has been demonstrated [10-13]. Previous studies reported that OVX might have no significant effect on the mandible [14, 15]. In fact, the mandible differs from the long bone both morphologically and functionally. Thus, the response of the mandible to OVX is not the same as that of the long bone. The mandibular alveolar bone has also been found to be less sensitive to OVX than long bones [16, 17]. Furthermore, the BMD and bone volume/total volume of the mandible decreases less significantly than the long bone in response to OVX; however, the specific mechanism of this phenomenon remains unclear. A recent study suggested that the mechanical loading of the alveolar process during mastication might protect the alveolar bone from the bone loss observed in other skeletal sites [16]. The irregular shape of the mandible and increased masticatory of the incisor and molar of OVX mice, which have been reported to eat approximately 10% more than the sham controls in alveolar bone [18], may possibly be important factors that contribute to these negative results. Furthermore, the mandible develops from the neuroectoderm, whereas the bone of the axial and appendicular skeleton arises from the mesoderm. This embryological difference may also be the cause for the difference in the sensitivity of the two skeletal sites to estrogen deficiency [16].

Accumulated evidence suggests that microRNAs (miRNAs) have an important role in regulating bone mass. In recent years, the role of miRNAs in the progress of osteoporosis has gained interest. Numerous studies demonstrated that the dysregulation of miRNAs is associated with osteoporosis. MiR-2861 was found to affect osteoblast differentiation, contributing to osteoporosis in the femur via its effects on osteoblasts [19]. Transgenic mice overexpressing miR-34c exhibit low bone mass in both long bones and vertebrae, which are involved in the regulation of osteoblastogenesis by targeting multiple components of the Notch signaling pathway [20]. In addition, miR-21 is significantly down-regulated [21], whereas miR-3077-5p and miR-705 are significantly enhanced [22] in the mesenchymal stem cell derived from estrogen deficiency-induced osteoporosis. Most recently, Wang et al. found that miR-214 level is elevated in bone specimens from aged patients with fractures. Furthermore, miR-214 has a crucial role in suppressing bone formation by directly targeting the activating transcription factor 4 (ATF4) [23]. MiR-210 has been reported to ameliorate the estrogen deficiency-caused postmenopausal osteoporosis by promoting VEGF expression and osteoblast differentiation [24, 25]. More importantly, investigations on miRNAs expression profiles in femurs using ovariectomized mice model have shown that eight miRNAs (i.e., miR-127,-133a,-133a*,-133b,-136,-206,-378,-378*) are up-regulated after OVX, whereas one miRNA (i.e., miR-204) is down-regulated [26]. All these studies have confirmed the fundamental function of miRNAs in osteoporosis in long bones. However, studies on the role of miRNA in mandibular osteoporosis remain limited and unclear. Only recently, a study on the mechanism of the anti-osteopenic effect of Rhizoma Dioscoreae in alveolar bone suggested that miRNA regulation is involved in mandibular [27]. Considering the difference between the mandible and long bones, we believe that the miRNA regulation in mandibular osteoporosis possibly differs from that in long bones.

This study investigates the changes in the miRNA expression profiling of the mandible in OVX-induced osteoporosis mouse model using microarray analysis. We also analyze the specific miRNA-mRNA-function complex network and signaling pathways in the regulation of osteoporosis in the mandible by comparing the differentially expressed miRNAs (DEmiRs) and their validated target gene data from the mandible and femur.

Materials and Methods

Animals

Female C57BL/6 mouse aged 8 weeks (mean weight of 19 g) were purchased from Slaccas Laboratory Animal Corporation (Shanghai, China). The mice had access to food and water ad libitum. The mice were anesthetized with an intraperitoneal injection of chloral hydrate (10%, 4 ml/kg body weight). Bilateral OVX (n = 8) or sham operation (Sham-op, n = 8) was performed following the standard method [12]. All the mice were kept in cages under standard laboratory conditions and fed standard chow during the course of the experiments. After 12 weeks, all the mice were weighed and prepared for the following experiments.

Preparation of Specimen

A total of 12 weeks after surgery, the animals were anesthetized with an intraperitoneal injection of chloral hydrate (10%, 4 ml/kg body weight). The right mandible and femur were dissected, filled with 4% paraformaldehyde for two days at room temperature, and then stored in 0.5% paraformaldehyde at 4°C for the measurements of BMD and microstructure by micro-computerized tomography (micro-CT). After the measurement of micro-CT, the right mandibles were used for histological analysis. In the case of the left mandibles, we initially extracted the molars and most of the incisor, and then dissected the whole mandible for microarray and real-time quantitative RT-PCR assays.

Micro-CT and Histological Analysis

The right mandibles and femurs of the mice (n = 3), without sample preparation or decalcification, were scanned with a high-resolution micro-CT (SkyScan1076, Bruker micro-CT, USA). The specimens were analyzed with the software SkyScan CTVOX 2.1. Image acquisition of the femur was performed at energy of 40 kV and intensity of 250 μA with a voxel size of 18 μm. Image acquisition of the mandible was performed with a voxel size of 8.8 μm. Once the micro-CT analysis was completed, the samples were ready for histological analysis. After decalcification, the samples of the mandible and femur were gradient-dehydrated and embedded in paraffin. Serial sections of 4 μm were cut and then stained with H&E in accordance with the manufacturer's protocol.

RNA extraction and array analysis

The mandible was prepared from sham-operated mice and OVX mice. The left mandible from the sham-operated group and OVX group were harvested using TRIzol (Sigma-Aldrich) to extract the total RNA. The total RNA was quantified with NanoDrop ND-2100 (Thermo Scientific), and RNA integrity was assessed using Agilent 2100 (Agilent Technologies). Sample labeling, microarray hybridization, and washing were performed based on the manufacturer's standard protocols. Briefly, the total RNA was tailed with Poly A and then labeled with Biotin. Afterward, the labeled RNAs were hybridized on the microarray. After washing and staining the slides, the arrays were scanned with Affymetrix Scanner 3000 (Affymetrix). The software Affymetrix GeneChip Command Console (version4.0, Affymetrix) was used to analyze the array images to obtain raw data and then conduct RMA normalization. Next, Genespring software (version 12.5; Agilent Technologies) was used to conduct the subsequent data analysis.

MiRNA expression analysis and miRNA targets

We used the fold change method to select the DEmiRs from the OVX and sham-operated control mice, and the miRNAs with |log 2(fold change)|>1.0 were considered to be the DEmiRs. In this study, three databases (i.e., TarBase [28], miRTarBase [29], and miRecords [30]) were used to screen the experiment-confirmed significant target genes of DEmiRs. After integrating the data from the three databases, we utilized the Cytoscape 2.8.3 software to generate the miRNA-mRNA regulation network. Through the plugin "Network Analysis" of Cytoscape, we further extracted the network topological characteristics of DEmiRs in the regulation network. The topological characteristics included degree, average shortest path length, closeness centrality, betweenness centrality, and topological coefficient. According to these topological characteristics, we further explored the vital miRNAs in the OVX mice.

MiRNA-mRNA-function complex network

To obtain a better understanding of the biological function of the miRNAs dysregulated in OVX, we applied the online tool of Database for Annotation, Visualization and Integrated Discovery (DAVID) v6.7 to analyze the biological functions of the miRNA target genes. DAVID bioinformatics resources consist of an

integrated biological knowledgebase and provide a comprehensive set of functional annotation tools for investigators to understand the biological meaning from large gene lists [31]. Here, we analyzed the roles of miRNA from three aspects of gene ontology [32], namely, biological process, molecular function, and cellular component (i.e., the p value and FDR cut-offs were 0.05). Moreover, based on the Kyoto Encyclopedia of Genes and Genomes (KEGG), we explored the significant pathways in which DEmiRs are involved (i.e., the p-value cut-off is 0.05). By integrating the miRNA-mRNA regulation network with pathway-enriched target pairs, we further constructed the miRNA-mRNA-pathway complex network. According to the complex network, we directly exhibited the relationships among miRNA, mRNA, and pathways and derived the potential risk of miRNAs.

Statistical Analysis

All the values were expressed as mean ± standard deviation. All analyses were conducted using SPSS 20.0 (SPSS Inc., Chicago, IL, USA). The difference between the evaluated parameters in the groups was tested using two independent-samples t tests. $P < 0.05$ was considered to be statistically significant.

Results

Establishment of estrogen deficiency–induced osteoporosis mice model

The mice were weighted 12 weeks after surgery, and the mean weight of the OVX group was significantly heavier than that of the sham-operated group (Fig. 1A). Micro-CT images and histological sections were used to visualize the establishment of the osteoporotic model (Fig. 1). Compared with those of the sham-operated mice, the 3D images of the femur in the OVX group showed a significant decrease in the subchondral trabecular bone volume, thickness, and density (Fig. 1B). The 2D images showed the same results as the 3D images (Fig. 1C). The H&E staining of the distal femur in the two groups also showed a significant decrease in subchondral trabecular bone volume in the OVX group compared with the sham-operated group (Fig. 1D). Analysis of the micro-CT data of the femur demonstrated a significant decrease in BMD, bone volume over total volume (BV/TV), and trabecular number, and an increase in bone surface over bone volume compared with data of the sham-operated group (Table 1), which is consistent with the histological results.

In this study, the mandible of the OVX mice was compared with that of the sham-operated mice. The results from the 3D images of the OVX mice showed a significant decrease in the alveolar bone compared with those from the sham-operated mice (Fig. 2A). The results of the 2D images confirmed osteoporosis in the mandible of the OVX animals from the coronal, sagittal, and transaxial slice (Fig. 2B). The OVX mice showed an obvious decrease in the alveolar bone of the first molar compared with the sham-operated mice, especially the alveolar bone offurcation (Fig. 2B). Moreover, the H&E staining of the alveolar bone of the first molar from OVX group showed a significant decrease in furcation and a relatively scant marrow space compared with that of the sham-operated group, which is consistent with the results of the micro-CT (Fig. 2C). The alveolar bone and basal bone of the mandible were also analyzed. The micro-CT data of the mandible of OVX mice demonstrated a significant decrease in BMD and BV/TV (Fig. 2D).

MiRNA expression analysis

The miRNA expression profiles of the OVX and sham-operated groups were determined using miRNA microarray analysis. The expressed miRNA data were normalized through median normalization. To identify DEmiRs, the restriction criteria $|\log2 \text{ (fold change)}| > 1.0$ was applied. The results showed 53 DEmiRs, including 18 up-regulated miRNAs and 35 down-regulated miRNAs in OVX mice compared with sham-operated mice (Fig. 3 and Table 3).

Functional analysis

To better understand the biological role of these DEmiRs in the mandible of mice after OVX, three databases were used to screen the confirmed significant target genes of miRNAs

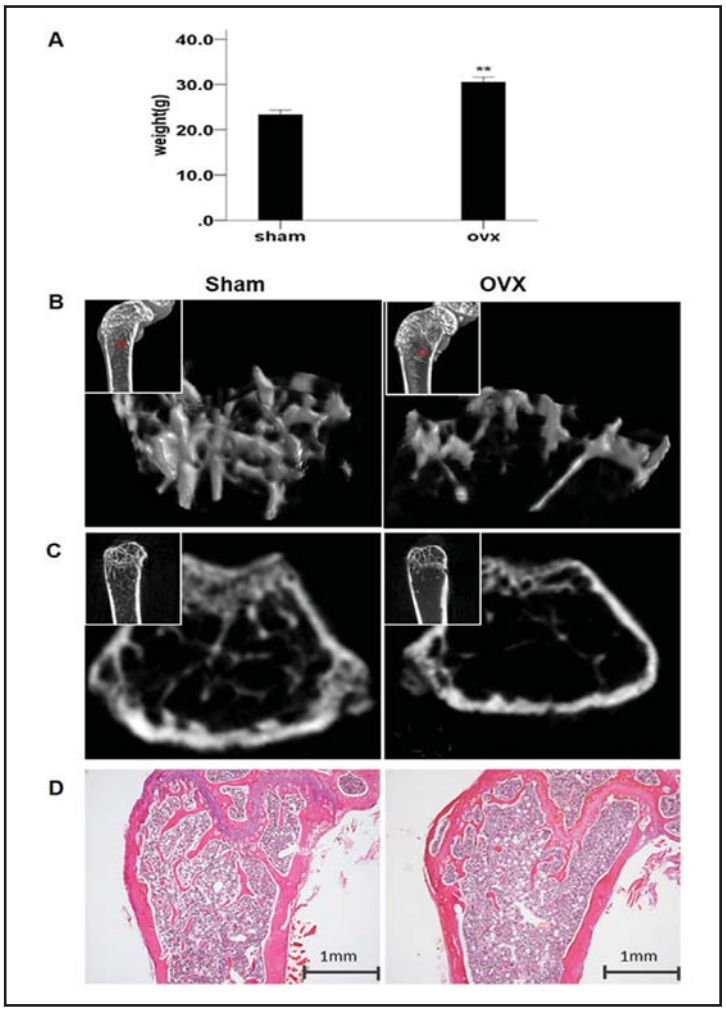

Fig. 1. Establishment of the mouse osteoporotic model. (A) The mean body-weight of the OVX group and sham-operated group. (B) 3D images of the femur head in the bone of the sham-operated and OVX groups. (C) 2D images of the femur head in the bone of the sham-operated and OVX groups. (D) Representative H&E staining for the femurs of the sham-operated and OVX groups (magnification 40x). ** $p < 0.01$.

using Cytoscape 2.8.3 software as described in the Materials and Method section. The screen results showed that 719 validated miRNA-target pairs were obtained, including 666 genes (Table 4) and 15 DEmiRs (Table 2), which indicated that these genes were the experimental validated targets of these 15 DEmiRs. By contrast, the rest of the 53 known DEmiRs in the mandible of OVX mice were not found in any of these databases. Function enrichment analysis was further conducted on these 666 genes with the online tool of DAVID (Fig. 4a–c). The results indicated that these 666 target genes of the miRNAs regulated many biological processes in the mandible of mice, including blood vessel development, vasculature development, regulation of transcription, regulation of macromolecule biosynthetic process, osteoblast differentiation, and muscle organ development (Fig. 4a). These target genes were associated with the cellular components of the axon, intracellular organelle, nucleus, actomyosin, and actin cytoskeleton (Fig. 4b). Moreover, these target genes of the DEmiRs also had a role in transition metal ion binding, protein kinase binding, protein kinase activity, calcium ion binding, and microtubule binding (Fig. 4c).

Table 1. Results from micro-CT analysis data of the femur between the OVX and Sham-operation group. Bone Volume over Total Volume (BV/TV), Bone Surface /Bone Volume (BS/BV), trabecular number (Tb.N). * $p < 0.05$

	Sham	OVX
BMD (g/cc)	0.33±0.13	0.25±0.11*
BV/TV (%)	21.17±1.34	8.24±2.01*
BS/BV (1/mm)	41.14±0.78	47.23±0.53*
Tb.N (1/mm)	2.07±0.08	0.78±0.19*

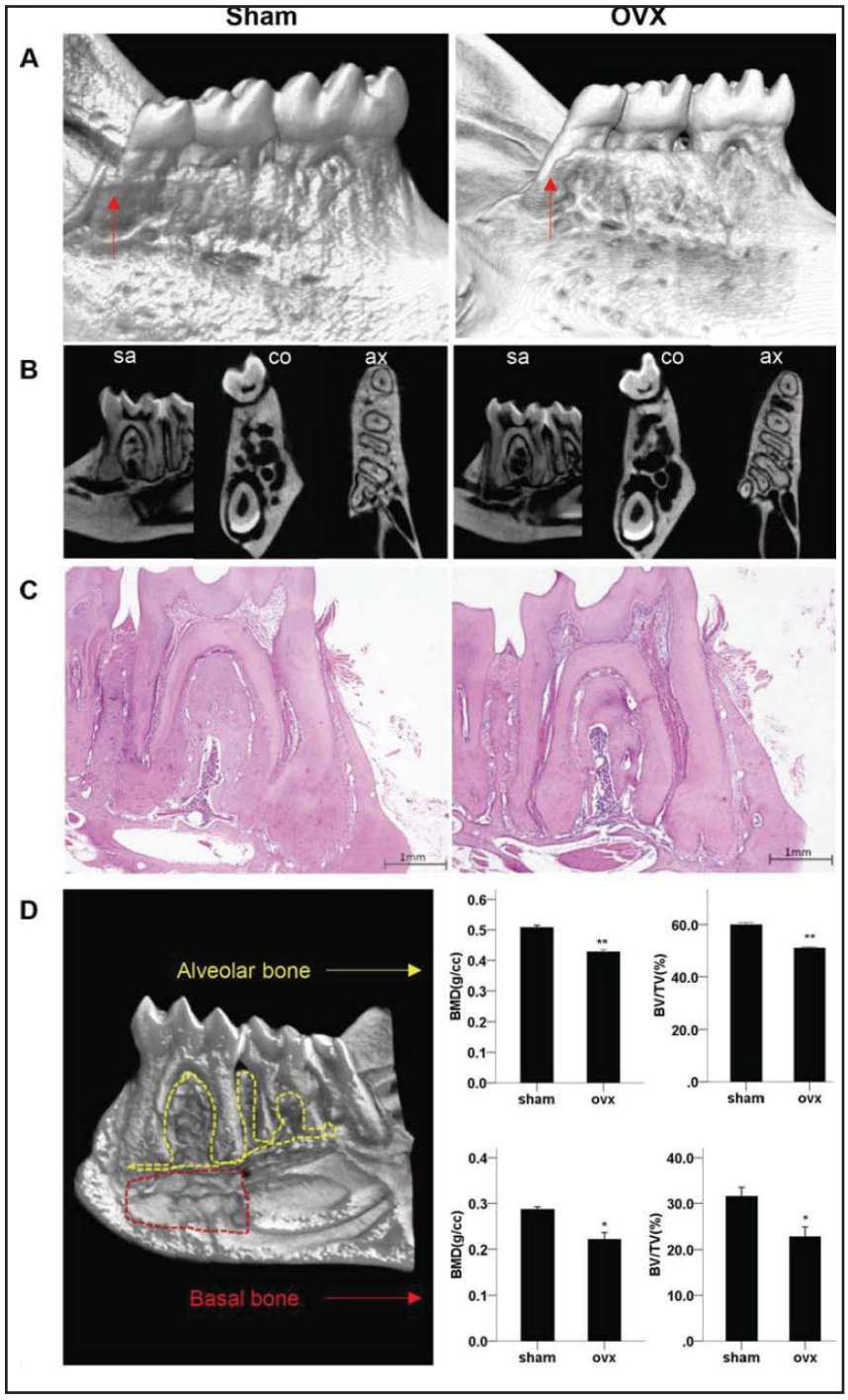

Fig. 2. OVX induced the mandibular osteoporosis. (A) 3D reconstruction of the mandible. Arrows show the loss of the alveolar bone in the sham-opreated mice vs OVX mice. (B) 2D images of microcomputed tomography. Sagittal slice ("sa"), coronal slice ("co"), and axial slice ("ax") in the alveolar bone compartment. (C) H&E staining of the alveolar bone of the first molar. (D) 3D reconstruction of the region of interest of the alveolar bone and basal bone compartments. Results from the micro-CT of BMD and BV/TV in the alveolar and basal bone compartments. * $p < 0.05$,** $p < 0.01$.

To compare the development of osteoporosis in the mandible with that in the femur in OVX mice, we extracted the data of the DEmiRs from the research conducted by An et al. [26]. A total of 8 miRNAs were up-regulated (i.e., miR-127, -133a-5p, -133a-3p,-133b,-136, -206, -378, -378-3p), whereas one miRNA (i.e., miR-204) was down-regulated. Using the same strategy, these eight DEmiRs were integrated with the three databases for screening. The results indicated that 27 validated miRNA-target pairs were acquired, including 22 genes and 5 DEmiRs (see Table 5), which suggested that these 22 genes were the validated targets of the 5 DEmiRs. Function enrichment analysis demonstrated that these 22 target genes of DEmiRs in the femur of OVX mice had important roles in many biological processes, such as the

generation of neurons, cell morphogenesis, and skeletal muscle organ development (Fig. 4d).

The miRNA-mRNA-pathway complex network

To better understand the biological function of DEmiRs in OVX mice, we applied the online tool of DAVID to analyze the interaction of DEmiRs with the biological functions of their target genes. A total of 719 experimentally validated miRNA-target pairs were used, including 666 genes and 15 DEmiRs (Fig. 5a). The topological characteristics of the network of DEmiRs and their target genes were calculated (Table 2). In this network, higher-degree nodes were more pivotal than the lower-degree nodes for robustness of the network, and the higher-degree nodes influenced more biological functions. Thus, the nodes with the highest degree were selected as the potential risk biomarkers. In this study, mmu-miR-17-5p was found to have the highest degree, and mmu-miR-297a-5p the second highest.

In addition, the significant pathways in which the target genes of DEmiRs were involved in the mandible were further explored based on the KEGG database. Finally, the enriched pathways were integrated into the miRNA-mRNA network, and the miRNA-mRNA-pathway complex network was finally constructed (Fig. 5a). The final miRNA-mRNA-pathway complex network clearly demonstrated that mmu-miR-17-5p and mmu-

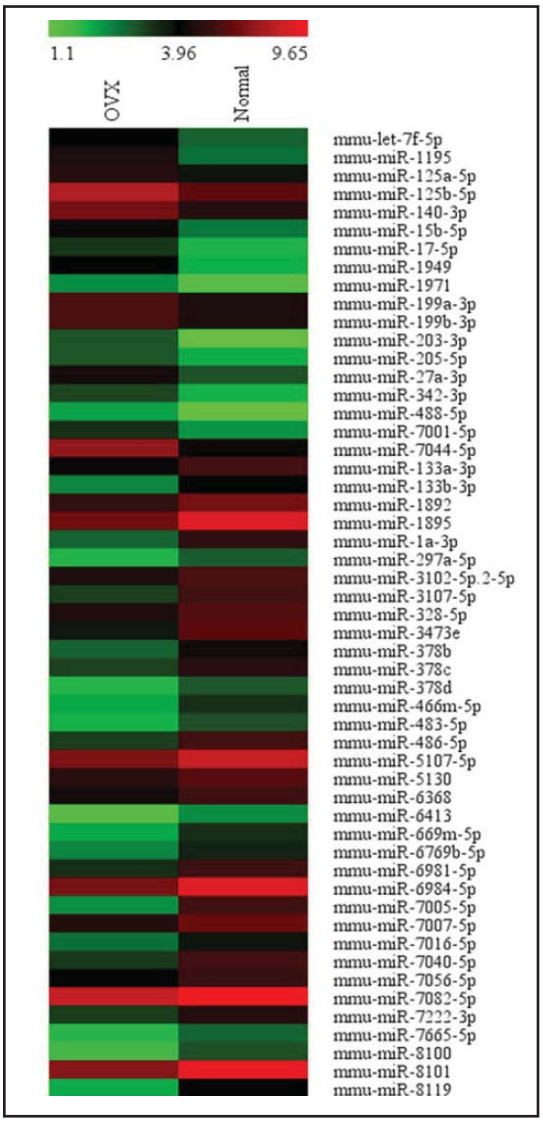

Fig. 3. Heatmap of the DEmiRs in the OVX and sham-operated groups. Results of the miRNA expression profile analysis showed 53 different expressed miRNAs (DEmiRs), including 18 up-regulated miRNAs and 35 down-regulated miRNAs in OVX mice compared with sham-operated mice. The colors from green to red represent the higher to lower expression levels of miRNAs.

Table 2. The topological characteristics of DEmiRs in miRNA-mRNA interaction network

miRNA	Degree	Average Shortest Path Length	Betweenness Centrality	Closeness Centrality	Topological Coefficient
mmu-miR-17-5p	377	1.87386	0.848769	0.533658	0.022812
mmu-miR-297a-5p	252	2.454407	0.546643	0.40743	0.150794
mmu-miR-1a-3p	28	3.651976	0.099399	0.273824	0.107143
mmu-miR-125b-5p	25	3.709726	0.077498	0.269562	0.06
mmu-miR-133a-3p	13	5.588146	0.021214	0.17895	0.461538
mmu-miR-199a-3p	4	1.875	0.642857	0.533333	0.25
mmu-miR-27a-3p	4	1.875	0.642857	0.533333	0.25
mmu-miR-125a-5p	3	5.694529	0.003042	0.175607	0.666667
mmu-miR-486-5p	3	3.746201	0.004162	0.266937	0.333333
mmu-miR-133b-3p	2	1	1	1	0
mmu-miR-203-3p	2	1	1	1	0
mmu-miR-15b-5p	1	1	0	1	0
mmu-miR-199b-3p	1	1	0	1	0
mmu-miR-205-5p	1	3.852584	0.00304	0.259566	0.5
mmu-miR-483-5p	1	1	0	1	0

Table 3. Fifty-three differentially expressed miRNAs comparing the OVX with sham-operation control mice

miRNA_name	Log FC ([OVX] vs [Normal])	Alignments	Sequence
mmu-miR-7044-5p	2.986956	chr6:118085197-118085215 (+)	GUGUGGUGGUGGUGGCGGC
mmu-miR-1949	2.050919	chr18:35554612-35554635 (+)	CUAUACCAGGAUGUCAGCAUAGUU
mmu-miR-203-3p	1.885073	chr12:112130927-112130948 (+)	GUGAAAUGUUUAGGACCACUAG
mmu-miR-1195	1.856476	chr17:70860558-70860580 (-)	UGAGUUCGAGGCCAGCCUGCUCA
mmu-miR-140-3p	1.800233	chr8:107551288-107551308 (+)	UACCACAGGGUAGAACCACGG
mmu-miR-125b-5p	1.792335	chr16:77646279-77646300 (+) //chr9:41581940-41581961(+)	UCCCUGAGACCCUAACUUGUGA
mmu-miR-15b-5p	1.585078	chr3:69009775-69009796 (+)	UAGCAGCACAUCAUGGUUUACA
mmu-miR-17-5p	1.466469	chr14:115043684-115043706 (+)	CAAAGUGCUUACAGUGCAGGUAG
mmu-miR-27a-3p	1.36949	chr8:84208727-84208747 (+)	UUCACAGUGGCUAAGUUCCGC
mmu-miR-342-3p	1.249035	chr12:108658680-108658702 (+)	UCUCACACAGAAAUCGCACCCGU
mmu-let-7f-5p	1.184503	chr13:48537889-48537910 (-) // chrX:151912353-151912374 (+)	UGAGGUAGUAGAUUGUAUAGUU
mmu-miR-199a-3p	1.183639	chr1:162217883-162217904 (+) // chr9:21496498-21496519 (-)	ACAGUAGUCUGCACAUUGGUUA
mmu-miR-199b-3p	1.183639	chr2:32318524-32318545 (+)	ACAGUAGUCUGCACAUUGGUUA
mmu-miR-7001-5p	1.128903	chr2:93421980-93422002 (-)	AGGCAGGGUGUGAGCGUGAGCAU
mmu-miR-1971	1.054252	chr14:78191451-78191468 (-)	GUAAAGGCUGGGCUGAGA
mmu-miR-125a-5p	1.031875	chr17:17830817-17830840 (+)	UCCCUGAGACCCUUUAACCUGUGA
mmu-miR-205-5p	1.024269	chr1:193507503-193507524 (-)	UCCUUCAUUCCACCGGAGUCUG
mmu-miR-488-5p	1.021523	chr1:158505651-158505671 (+)	CCCAGAUAAUAGCACUCUCAA
mmu-miR-7665-5p	-1.02529	chr2:120017517-120017539 (+)	AAGGGAAGGCAGGAGAAAGGCUG
mmu-miR-297a-5p	-1.06808	chr2:10472264-10472285 (+) //chr2:10515830-10515851 (+) //chr2:10517077-10517098 (+) // chr7:10958477-10958498 (-)	AUGUAUGUGUGCAUGUGCAUGU
mmu-miR-6413	-1.08031	chr10:20297593-20297613 (-)	UGGCUCAGAAGAGCAGGUAGU
mmu-miR-5130	-1.09011	chr14:102982608-102982631 (-)	CUGGAGCGCGCGGGGCGAGGCAGGC
mmu-miR-7016-5p	-1.09676	chr4:129684546-129684566 (-)	CAGGGAGGGGAGCGAGAGUAG
mmu-miR-6368	-1.12334	chr13:28710796-28710816 (-)	CUGGGAAGCAGUGGAGGGGAG
mmu-miR-6769b-5p	-1.12438	chr8:71631083-71631102 (-)	CCUGGUGGGUGGGGAAGAGC
mmu-miR-3102-5p.2-5p	-1.14533	chr7:100882367-100882387 (-)	GGUGGUGCAGGCAGGAGAGCC
mmu-miR-378d	-1.14804	chr10:126710355-126710376 (-)	ACUGGCCUUGGAGUCAGAAGGU
mmu-miR-483-5p	-1.14804	chr7:142654968-142654989 (-)	AAGACGGGAGAAGAGAAGGGAG
mmu-miR-7082-5p	-1.231	chr9:21075563-21075583 (-)	UACGGGCAGGAGGAGGGGAGG
mmu-miR-328-5p	-1.28719	chr8:105308419-105308440 (-)	GGGGGGCAGGAGGGGCUCAGGG
mmu-miR-669m-5p	-1.35694	chr2:10512814-10512836 (+) // chr2:10513457-10513479 (+)	UGUGUGCAUGUGCAUGUGUGUAU
mmu-miR-466m-5p	-1.35694	chr2:10466677-10466699 (+)	UGUGUGCAUGUGCAUGUGUGUAU
mmu-miR-133a-3p	-1.39556	chr18:10782913-10782934 (-) // chr2:180398437-180398458 (+)	UUUGGUCCCCUUCAACCAGCUG
mmu-miR-1892	-1.42337	chr12:54645943-54645964 (-)	AUUUGGGGACGGGAGGGAGGAU
mmu-miR-7056-5p	-1.43437	chr7:47083203-47083224 (-)	UGUGGAGGAGGACAGAGAGGUU
mmu-miR-8100	-1.43584	chr11:46102300-46102322 (+)	AGGAGGAAAGGGAGCAAGCAGGU
mmu-miR-378b	-1.45216	chr11:88352839-88352858 (+)	CUGGACUUGGAGUCAGAAGA
mmu-miR-133b-3p	-1.47233	chr1:20682834-20682855 (+)	UUUGGUCCCCUUCAACCAGCUA
mmu-miR-7222-3p	-1.58296	chr2:92594654-92594676 (+)	UCCAGGACAGUGGGCAGGAGCAG
mmu-miR-7007-5p	-1.58835	chr3:20222332-20222354 (-)	UCAGAAGAGGCAGUGGAGGAGAU
mmu-miR-5107-5p	-1.66668	chr18:60812086-60812106 (+)	UGGGCAGAGGAGGCAGGGACA
mmu-miR-378c	-1.71938	chr14:46954905-46954925 (-)	ACUGGACUUGGAGUCAGAAGC
mmu-miR-8119	-1.94067	chr4:129557756-129557775 (-)	GAGGAGAGGGAGCUAGGGUC
mmu-miR-6981-5p	-2.08335	chr18:37974592-37974617 (-)	GUGAGGAGAAGGAAGAGGCUGAAGGC
mmu-miR-8101	-2.15189	chr11:102230103-102230124 (-)	GGCGAGCGGAGCCGGAGGAGCC
mmu-miR-1a-3p	-2.24766	chr18:10785485-10785506 (-) // chr2:180389096-180389117 (+)	UGGAAUGUAAAGAAGUAUGUAU
mmu-miR-6984-5p	-2.28393	chr19:3288925-3288948 (+)	ACUGAAAGGCAAUGAAGGAGGAGC
mmu-miR-7040-5p	-2.28965	chr6:83049716-83049737 (+)	CAUACGGAGGGAGAUGGAGGCG
mmu-miR-3473e	-2.33734	chr5:31667296-31667316 (-)	GGGCUGGAGAGAUGGCUCGUA
mmu-miR-486-5p	-2.34895	chr8:23142587-23142608 (+)	UCCUGUACUGAGCUGCCCCGAG
mmu-miR-3107-5p	-2.34895	chr8:23142627-23142648 (-)	UCCUGUACUGAGCUGCCCCGAG
mmu-miR-1895	-2.46713	chr3:134240515-134240536 (-)	CCCCCGAGGAGGACGAGGAGGA
mmu-miR-7005-5p	-3.17313	chr2:180179797-180179818 (-)	CCUGGGGAUGGGAGGACCAGCA

miR-297a-5p significantly influenced the biological pathways and were considered to be potential biomarkers in the development of the mandible of OVX mice.

Moreover, the miRNA-mRNA-pathway complex network of the 5 DEmiRs and their 22 target genes in the femurs of OVX mice was also constructed with the same previous strategy (i.e., Fig. 5b, data extracted from An et al. [26]). As demonstrated by the complex network, mmu-miR-133a-5p and mmu-miR-133a-3p significantly influenced the biological pathways and were considered to be potential biomarkers in the development of femur of OVX mice.

As shown in the Fig. 5a, the DEmiRs and their validated target genes were mainly involved in the T-cell receptor-signaling pathway, VEGF signaling pathway, Wnt signaling pathway,

Table 4. The 719 validated miRNA-target pairs, including 666 genes and 15 DEmiRs in mandible

miRNA	Target gene	miRNA	Target gene	miRNA	Target gene
mmu-miR-125a-5p	Cbx7	mmu-miR-17-5p	Cacna2d1	mmu-miR-297a-5p	Chd7
mmu-miR-125a-5p	Trim71	mmu-miR-17-5p	Capn2	mmu-miR-297a-5p	Akap9
mmu-miR-125a-5p	4632428N05Rik	mmu-miR-17-5p	Cav1	mmu-miR-297a-5p	Atp8b2
mmu-miR-125b-5p	Igf2	mmu-miR-17-5p	Cbx2	mmu-miR-297a-5p	Zfp108
mmu-miR-125b-5p	4632428N05Rik	mmu-miR-17-5p	Cdc7	mmu-miR-297a-5p	Slc1a4
mmu-miR-125b-5p	Bmf	mmu-miR-17-5p	Cdh2	mmu-miR-297a-5p	Pcdh17
mmu-miR-125b-5p	Arid3b	mmu-miR-17-5p	Chl1	mmu-miR-297a-5p	4931406P16Rik
mmu-miR-125b-5p	Abtb1	mmu-miR-17-5p	Col4a2	mmu-miR-297a-5p	Gltp
mmu-miR-125b-5p	Rhebl1	mmu-miR-17-5p	Cops2	mmu-miR-297a-5p	Cyb561d2
mmu-miR-125b-5p	Suv39h1	mmu-miR-17-5p	Cpe	mmu-miR-297a-5p	Zscan22
mmu-miR-125b-5p	Ajuba	mmu-miR-17-5p	Dpysl2	mmu-miR-297a-5p	Vps39
mmu-miR-125b-5p	Lin28a	mmu-miR-17-5p	Dio2	mmu-miR-297a-5p	Fut9
mmu-miR-125b-5p	Map2k7	mmu-miR-17-5p	Dmd	mmu-miR-297a-5p	Fzd1
mmu-miR-125b-5p	Entpd4	mmu-miR-17-5p	Dnmt3a	mmu-miR-297a-5p	Galnt3
mmu-miR-125b-5p	Rabl6	mmu-miR-17-5p	Eef2k	mmu-miR-297a-5p	Ostm1
mmu-miR-125b-5p	Snai1	mmu-miR-17-5p	En2	mmu-miR-297a-5p	Foxj1
mmu-miR-125b-5p	Klf13	mmu-miR-17-5p	Epha7	mmu-miR-297a-5p	Zfp697
mmu-miR-125b-5p	Trim71	mmu-miR-17-5p	Eps15	mmu-miR-297a-5p	Pde5a
mmu-miR-125b-5p	Arid3a	mmu-miR-17-5p	Erbb4	mmu-miR-297a-5p	Fam110b
mmu-miR-125b-5p	Ddx19b	mmu-miR-17-5p	Celf2	mmu-miR-297a-5p	Rsbn1l
mmu-miR-125b-5p	Tor2a	mmu-miR-17-5p	Ezh1	mmu-miR-297a-5p	Slc29a4
mmu-miR-125b-5p	Dus1l	mmu-miR-17-5p	F3	mmu-miR-297a-5p	Tmem255a
mmu-miR-125b-5p	Ppt2	mmu-miR-17-5p	Fn1	mmu-miR-297a-5p	Srgap3
mmu-miR-125b-5p	Cbfb	mmu-miR-17-5p	Gabra1	mmu-miR-297a-5p	Zfp652
mmu-miR-125b-5p	Smo	mmu-miR-17-5p	Gabrb3	mmu-miR-297a-5p	Robo2
mmu-miR-125b-5p	Apln	mmu-miR-17-5p	B4galnt1	mmu-miR-297a-5p	Macf1
mmu-miR-125b-5p	Tnf	mmu-miR-17-5p	Gas7	mmu-miR-297a-5p	Adam10
mmu-miR-125b-5p	Zfp385a	mmu-miR-17-5p	Gng4	mmu-miR-297a-5p	Adam12
mmu-miR-133a-3p	Rhoa	mmu-miR-17-5p	Gpm6b	mmu-miR-297a-5p	Add1
mmu-miR-133a-3p	Nfatc4	mmu-miR-17-5p	Grb10	mmu-miR-297a-5p	Ank3
mmu-miR-133a-3p	Pola1	mmu-miR-17-5p	Trip12	mmu-miR-297a-5p	Xiap
mmu-miR-133a-3p	Hdac4	mmu-miR-17-5p	Hsd17b10	mmu-miR-297a-5p	Nr2f2
mmu-miR-133a-3p	Nelfa	mmu-miR-17-5p	Smim20	mmu-miR-297a-5p	Arf2
mmu-miR-133a-3p	Runx2	mmu-miR-17-5p	Ajuba	mmu-miR-297a-5p	Atrn
mmu-miR-133a-3p	Igf1r	mmu-miR-17-5p	Kif21a	mmu-miR-297a-5p	Cab39
mmu-miR-133a-3p	Ucp2	mmu-miR-17-5p	Kif5a	mmu-miR-297a-5p	Capn2
mmu-miR-133a-3p	Spry1	mmu-miR-17-5p	Kif5c	mmu-miR-297a-5p	Cav1
mmu-miR-133a-3p	Cdc42	mmu-miR-17-5p	Klf9	mmu-miR-297a-5p	Cav2
mmu-miR-133a-3p	Ccnd2	mmu-miR-17-5p	Kras	mmu-miR-297a-5p	Cct2
mmu-miR-133a-3p	Casp9	mmu-miR-17-5p	Lrrn3	mmu-miR-297a-5p	Cdh11
mmu-miR-133a-3p	Srf	mmu-miR-17-5p	M6pr	mmu-miR-297a-5p	Cfl2
mmu-miR-133b-3p	Pitx3	mmu-miR-17-5p	Mcl1	mmu-miR-297a-5p	Clk1
mmu-miR-133b-3p	Ptbp2	mmu-miR-17-5p	Mcm7	mmu-miR-297a-5p	Cplx2
mmu-miR-15b-5p	Arl2	mmu-miR-17-5p	Mrc1	mmu-miR-297a-5p	Ncan
mmu-miR-17-5p	App	mmu-miR-17-5p	Map1a	mmu-miR-297a-5p	Celf1
mmu-miR-17-5p	Cpeb4	mmu-miR-17-5p	Map2	mmu-miR-297a-5p	Dhx9
mmu-miR-17-5p	Adcyap1r1	mmu-miR-17-5p	Map4	mmu-miR-297a-5p	Dio2
mmu-miR-17-5p	Anp32a	mmu-miR-17-5p	Myo10	mmu-miR-297a-5p	Elk3
mmu-miR-17-5p	Ap3d1	mmu-miR-17-5p	Napb	mmu-miR-297a-5p	Epb4.1l1
mmu-miR-17-5p	Aplp2	mmu-miR-17-5p	Ncam1	mmu-miR-297a-5p	Celf2
mmu-miR-17-5p	Slc36a1	mmu-miR-17-5p	Neurod1	mmu-miR-297a-5p	Fgf11
mmu-miR-17-5p	Nsg2	mmu-miR-17-5p	Nf1	mmu-miR-297a-5p	Ctgf
mmu-miR-17-5p	Oprl1	mmu-miR-17-5p	Nfe2l2	mmu-miR-297a-5p	Fmn1
mmu-miR-17-5p	Pappa	mmu-miR-17-5p	Nfia	mmu-miR-297a-5p	Otud4
mmu-miR-17-5p	Nptx1	mmu-miR-17-5p	Hdac8	mmu-miR-297a-5p	Paqr8
mmu-miR-17-5p	Tmod2	mmu-miR-17-5p	Draxin	mmu-miR-297a-5p	Gorasp1
mmu-miR-17-5p	Zfhx3	mmu-miR-17-5p	Tmem230	mmu-miR-297a-5p	Neto2
mmu-miR-17-5p	Atf2	mmu-miR-17-5p	Rasgef1a	mmu-miR-297a-5p	Mettl5
mmu-miR-17-5p	Spast	mmu-miR-17-5p	Pfn2	mmu-miR-297a-5p	Idnk
mmu-miR-17-5p	Abca1	mmu-miR-17-5p	Plxna2	mmu-miR-297a-5p	Klhl24
mmu-miR-17-5p	Macf1	mmu-miR-17-5p	Ppp3r1	mmu-miR-297a-5p	Slc24a2
mmu-miR-17-5p	Acvr1b	mmu-miR-17-5p	Cyth1	mmu-miR-297a-5p	Fam101b
mmu-miR-17-5p	Adam10	mmu-miR-17-5p	Pten	mmu-miR-297a-5p	Klhdc10
mmu-miR-17-5p	Adam17	mmu-miR-17-5p	Ptpn11	mmu-miR-297a-5p	Wsb1
mmu-miR-17-5p	Adam19	mmu-miR-17-5p	Ptprg	mmu-miR-297a-5p	Uck2
mmu-miR-17-5p	Cdc42se2	mmu-miR-17-5p	Ptprj	mmu-miR-297a-5p	Elovl4
mmu-miR-17-5p	Fam117b	mmu-miR-17-5p	Rab12	mmu-miR-297a-5p	Kcnk1
mmu-miR-17-5p	Slc17a7	mmu-miR-17-5p	Rab33b	mmu-miR-297a-5p	Kif1b
mmu-miR-17-5p	Ccser2	mmu-miR-17-5p	Ranbp2	mmu-miR-297a-5p	Lmnb1
mmu-miR-17-5p	Dcbld2	mmu-miR-17-5p	Rasal1	mmu-miR-297a-5p	Lss
mmu-miR-17-5p	1700052N19Rik	mmu-miR-17-5p	Rb1	mmu-miR-297a-5p	Mnt
mmu-miR-17-5p	Ppp1r21	mmu-miR-17-5p	Rbl2	mmu-miR-297a-5p	Mxi1
mmu-miR-17-5p	Otud4	mmu-miR-17-5p	Rdx	mmu-miR-297a-5p	Ncoa2
mmu-miR-17-5p	Dnm1l	mmu-miR-17-5p	Rev3l	mmu-miR-297a-5p	Nptx1
mmu-miR-17-5p	Msl1	mmu-miR-17-5p	Ralgds	mmu-miR-297a-5p	Oxtr
mmu-miR-17-5p	Ftsjd2	mmu-miR-17-5p	Rora	mmu-miR-297a-5p	Pbx3
mmu-miR-17-5p	Zdhhc16	mmu-miR-17-5p	Ryr2	mmu-miR-297a-5p	Pde6d
mmu-miR-17-5p	Ankrd9	mmu-miR-17-5p	Scn1a	mmu-miR-297a-5p	Pik3r1
mmu-miR-17-5p	Cyld	mmu-miR-17-5p	Scn8a	mmu-miR-297a-5p	Pik3r3
mmu-miR-17-5p	Zfp84	mmu-miR-17-5p	Scp2	mmu-miR-297a-5p	Pja1
mmu-miR-17-5p	Cds1	mmu-miR-17-5p	Cxcl12	mmu-miR-297a-5p	Prkcb
mmu-miR-17-5p	Pcf11	mmu-miR-17-5p	Sema3c	mmu-miR-297a-5p	Plaa
mmu-miR-17-5p	Dhcr24	mmu-miR-17-5p	Sepp1	mmu-miR-297a-5p	Ptprr
mmu-miR-17-5p	Etnk1	mmu-miR-17-5p	Shh	mmu-miR-297a-5p	Pura
mmu-miR-17-5p	Pik3r4	mmu-miR-17-5p	Ski	mmu-miR-297a-5p	Qk

continued

MAPK signaling pathway, pathogenic Escherichia coli infection, and adherens junction. A comparison of the different regulation pathways of DEmiRs in the mandible and femur of

miRNA	Target gene	miRNA	Target gene	miRNA	Target gene
mmu-miR-17-5p	Pank1	mmu-miR-17-5p	Skil	mmu-miR-297a-5p	Rad21
mmu-miR-17-5p	Rab30	mmu-miR-17-5p	Sox8	mmu-miR-297a-5p	Rasgrp1
mmu-miR-17-5p	Slc24a2	mmu-miR-17-5p	Sall3	mmu-miR-297a-5p	Rdx
mmu-miR-17-5p	Slc10a7	mmu-miR-17-5p	Serpinb9	mmu-miR-297a-5p	Robo1
mmu-miR-17-5p	Klhl2	mmu-miR-17-5p	Stat3	mmu-miR-297a-5p	S100b
mmu-miR-17-5p	Crebrf	mmu-miR-17-5p	Syt1	mmu-miR-297a-5p	Scd1
mmu-miR-17-5p	Wdr82	mmu-miR-17-5p	Ubtf	mmu-miR-297a-5p	Scd2
mmu-miR-17-5p	Heg1	mmu-miR-17-5p	Tex2	mmu-miR-297a-5p	Scn8a
mmu-miR-17-5p	Limch1	mmu-miR-17-5p	Tgfa	mmu-miR-297a-5p	Ski
mmu-miR-17-5p	Polq	mmu-miR-17-5p	Ift88	mmu-miR-297a-5p	Slc31a1
mmu-miR-17-5p	6030458C11Rik	mmu-miR-17-5p	Klf10	mmu-miR-297a-5p	Snap25
mmu-miR-17-5p	Yipf6	mmu-miR-17-5p	Tnks	mmu-miR-297a-5p	Son
mmu-miR-17-5p	2810055G20Rik	mmu-miR-17-5p	Ugcg	mmu-miR-297a-5p	Sos1
mmu-miR-17-5p	Msantd4	mmu-miR-17-5p	Wfs1	mmu-miR-297a-5p	Serpini1
mmu-miR-17-5p	Map7d2	mmu-miR-17-5p	Zmat3	mmu-miR-297a-5p	Slk
mmu-miR-17-5p	Acap2	mmu-miR-17-5p	Xpc	mmu-miR-297a-5p	Syngr3
mmu-miR-17-5p	Stxbp5	mmu-miR-17-5p	Yy1	mmu-miR-297a-5p	Tgfa
mmu-miR-17-5p	Igsf3	mmu-miR-17-5p	Rnf103	mmu-miR-297a-5p	Tgfbr1
mmu-miR-17-5p	Trim2	mmu-miR-17-5p	Zfp62	mmu-miR-297a-5p	Klhdc8a
mmu-miR-17-5p	Pum1	mmu-miR-17-5p	Zic2	mmu-miR-297a-5p	Tgoln1
mmu-miR-17-5p	Gpr63	mmu-miR-17-5p	Akt3	mmu-miR-297a-5p	Ugt8a
mmu-miR-17-5p	Ankrd17	mmu-miR-17-5p	Gtf2h2	mmu-miR-297a-5p	Ulk1
mmu-miR-17-5p	Entpd7	mmu-miR-17-5p	Mgll	mmu-miR-297a-5p	Vldlr
mmu-miR-17-5p	Pabpc5	mmu-miR-17-5p	Tenm4	mmu-miR-297a-5p	Zmat3
mmu-miR-17-5p	Aff4	mmu-miR-17-5p	Xrn1	mmu-miR-297a-5p	Rnf103
mmu-miR-17-5p	Nipa2	mmu-miR-17-5p	Zeb2	mmu-miR-297a-5p	Zhx1
mmu-miR-17-5p	Brwd1	mmu-miR-17-5p	Map3k5	mmu-miR-297a-5p	Tenm2
mmu-miR-17-5p	Tnfrsf21	mmu-miR-17-5p	Map4k2	mmu-miR-297a-5p	Pde10a
mmu-miR-17-5p	Phlpp1	mmu-miR-17-5p	Mapk14	mmu-miR-297a-5p	Zfp260
mmu-miR-17-5p	Znfx1	mmu-miR-17-5p	Nbea	mmu-miR-297a-5p	Trp53bp1
mmu-miR-17-5p	Qser1	mmu-miR-17-5p	B3galt2	mmu-miR-297a-5p	Tceb3
mmu-miR-17-5p	Camta1	mmu-miR-17-5p	Aifm1	mmu-miR-297a-5p	D4Wsu53e
mmu-miR-17-5p	Tmem64	mmu-miR-17-5p	St6galnac5	mmu-miR-297a-5p	Ccnc
mmu-miR-17-5p	Mapre3	mmu-miR-17-5p	Sh3d19	mmu-miR-297a-5p	Dlg3
mmu-miR-17-5p	Nt5dc3	mmu-miR-17-5p	Tceb3	mmu-miR-297a-5p	Vamp4
mmu-miR-17-5p	Aldh6a1	mmu-miR-17-5p	Amot	mmu-miR-297a-5p	Rabep1
mmu-miR-17-5p	Foxp1	mmu-miR-17-5p	D4Wsu53e	mmu-miR-297a-5p	Elovl2
mmu-miR-17-5p	Ccdc88a	mmu-miR-17-5p	Mga	mmu-miR-297a-5p	Azin1
mmu-miR-17-5p	Ankhd1	mmu-miR-17-5p	Rabgap1l	mmu-miR-297a-5p	Fmn2
mmu-miR-17-5p	Sobp	mmu-miR-17-5p	Igfbp7	mmu-miR-297a-5p	Fras1
mmu-miR-17-5p	Tspan9	mmu-miR-17-5p	Ppap2b	mmu-miR-297a-5p	Wnk1
mmu-miR-17-5p	Cald1	mmu-miR-17-5p	Fam134c	mmu-miR-297a-5p	Itfg1
mmu-miR-17-5p	Atxn3	mmu-miR-17-5p	Pvr	mmu-miR-297a-5p	Sulf2
mmu-miR-17-5p	Scn2a1	mmu-miR-17-5p	Reep1	mmu-miR-297a-5p	Rsf1
mmu-miR-17-5p	Derl2	mmu-miR-17-5p	Brms1l	mmu-miR-297a-5p	Psd3
mmu-miR-17-5p	Bmp2k	mmu-miR-17-5p	Tmx4	mmu-miR-297a-5p	B4galt6
mmu-miR-17-5p	Elovl6	mmu-miR-17-5p	Gramd1a	mmu-miR-297a-5p	Chp1
mmu-miR-17-5p	Zfp704	mmu-miR-17-5p	Cd164	mmu-miR-297a-5p	Cbln3
mmu-miR-17-5p	Fchsd2	mmu-miR-17-5p	Insm1	mmu-miR-297a-5p	Foxo3
mmu-miR-17-5p	Fam120c	mmu-miR-17-5p	Celsr2	mmu-miR-297a-5p	Gmeb1
mmu-miR-17-5p	Wdr37	mmu-miR-17-5p	Rcan3	mmu-miR-297a-5p	Ttyh1
mmu-miR-17-5p	A330021E22Rik	mmu-miR-17-5p	Socs6	mmu-miR-297a-5p	Sv2a
mmu-miR-17-5p	Mlxip	mmu-miR-17-5p	Extl3	mmu-miR-297a-5p	Sc4mol
mmu-miR-17-5p	Rsrc2	mmu-miR-17-5p	Plagl2	mmu-miR-297a-5p	Lyrm9
mmu-miR-17-5p	Cpeb3	mmu-miR-17-5p	Slc1a4	mmu-miR-297a-5p	Haus2
mmu-miR-17-5p	Tfe3	mmu-miR-17-5p	Srcin1	mmu-miR-297a-5p	Pbrm1
mmu-miR-17-5p	Tbc1d12	mmu-miR-17-5p	Mycbp	mmu-miR-297a-5p	Ssbp2
mmu-miR-17-5p	Nudcd3	mmu-miR-17-5p	Serinc1	mmu-miR-297a-5p	Dnajb4
mmu-miR-17-5p	Lcorl	mmu-miR-17-5p	Sh3bgrl	mmu-miR-297a-5p	Ccdc47
mmu-miR-17-5p	Slc35f3	mmu-miR-17-5p	Sez6l	mmu-miR-297a-5p	Tmem19
mmu-miR-17-5p	Lpp	mmu-miR-17-5p	Cend1	mmu-miR-297a-5p	Tbc1d19
mmu-miR-17-5p	D15Ertd621e	mmu-miR-17-5p	Extl2	mmu-miR-297a-5p	Cap2
mmu-miR-17-5p	Arap2	mmu-miR-17-5p	Smoc2	mmu-miR-297a-5p	Cltc
mmu-miR-17-5p	Rassf4	mmu-miR-17-5p	Itm2c	mmu-miR-297a-5p	Ccdc127
mmu-miR-17-5p	Nudt18	mmu-miR-17-5p	Dip2a	mmu-miR-297a-5p	Ssr3
mmu-miR-17-5p	Tnrc6b	mmu-miR-17-5p	Dpysl5	mmu-miR-297a-5p	Pdcl
mmu-miR-17-5p	Kpnb1	mmu-miR-17-5p	Rogdi	mmu-miR-297a-5p	Cpeb4
mmu-miR-17-5p	Appl2	mmu-miR-17-5p	Camk2n1	mmu-miR-297a-5p	Mansc1
mmu-miR-17-5p	9-Mar	mmu-miR-17-5p	Pgrmc2	mmu-miR-297a-5p	1600012H06Rik
mmu-miR-17-5p	Papolg	mmu-miR-17-5p	Rnf220	mmu-miR-297a-5p	Ppap2b
mmu-miR-17-5p	Taok1	mmu-miR-17-5p	Kdelr2	mmu-miR-297a-5p	Spire1
mmu-miR-17-5p	Hid1	mmu-miR-17-5p	Pbrm1	mmu-miR-297a-5p	Leprotl1
mmu-miR-17-5p	Ubxn2a	mmu-miR-17-5p	Polr3k	mmu-miR-297a-5p	Micu2
mmu-miR-17-5p	Mylip	mmu-miR-17-5p	Ttc14	mmu-miR-297a-5p	2810407C02Rik
mmu-miR-17-5p	Rasa1	mmu-miR-17-5p	Tomm34	mmu-miR-297a-5p	Nup35
mmu-miR-17-5p	Fcho2	mmu-miR-17-5p	Zfand4	mmu-miR-297a-5p	Scrn1
mmu-miR-17-5p	6-Mar	mmu-miR-17-5p	Rbl2 / p130	mmu-miR-297a-5p	Stambp
mmu-miR-17-5p	Fam49b	mmu-miR-17-5p	Luc7l3	mmu-miR-297a-5p	Tspan2
mmu-miR-17-5p	Pim3	mmu-miR-17-5p	Ppp6c	mmu-miR-297a-5p	Spag9
mmu-miR-17-5p	Gxylt1	mmu-miR-17-5p	1600012H06Rik	mmu-miR-297a-5p	P2ry12
mmu-miR-17-5p	Ankrd29	mmu-miR-17-5p	Eml1	mmu-miR-297a-5p	Ing3
mmu-miR-17-5p	Epb4.1l5	mmu-miR-17-5p	Ubr3	mmu-miR-297a-5p	Ankrd12
mmu-miR-17-5p	Klhl20	mmu-miR-17-5p	Sdccag3	mmu-miR-297a-5p	Lgr4
mmu-miR-17-5p	Fam134a	mmu-miR-17-5p	Lmbrd1	mmu-miR-297a-5p	Skiv2l2
mmu-miR-17-5p	Dgkd	mmu-miR-17-5p	Ttc9	mmu-miR-297a-5p	Kcnk10

continued

the OVX model shows that the transforming growth factor-β (TGF-β) signaling pathway was only regulated by the DEmiRs in the mandible but not in the femur (Fig. 6a), whereas the

miRNA	Target gene	miRNA	Target gene	miRNA	Target gene
mmu-miR-17-5p	Ppig	mmu-miR-17-5p	Lnp	mmu-miR-297a-5p	Tmem87b
mmu-miR-17-5p	Zfp217	mmu-miR-17-5p	Aspscr1	mmu-miR-297a-5p	Ccnt2
mmu-miR-17-5p	Ythdf3	mmu-miR-17-5p	Necab1	mmu-miR-297a-5p	Xpot
mmu-miR-17-5p	Syt11	mmu-miR-17-5p	4931406C07Rik	mmu-miR-297a-5p	Wdr13
mmu-miR-17-5p	Rap1gds1	mmu-miR-17-5p	Zfp597	mmu-miR-297a-5p	Arrb1
mmu-miR-17-5p	Megf9	mmu-miR-17-5p	2510009E07Rik	mmu-miR-297a-5p	Lims1
mmu-miR-17-5p	Cnot6l	mmu-miR-17-5p	Spag9	mmu-miR-297a-5p	Scn2a1
mmu-miR-17-5p	Ficd	mmu-miR-17-5p	4930506M07Rik	mmu-miR-297a-5p	Nudt19
mmu-miR-17-5p	Fbxo21	mmu-miR-17-5p	8-Mar	mmu-miR-297a-5p	Tgs1
mmu-miR-17-5p	Wnk1	mmu-miR-17-5p	Scara5	mmu-miR-297a-5p	Bmp2k
mmu-miR-17-5p	Klhl42	mmu-miR-17-5p	Fbxo9	mmu-miR-297a-5p	Mical3
mmu-miR-17-5p	Rsf1	mmu-miR-17-5p	Dhx36	mmu-miR-297a-5p	Shank2
mmu-miR-17-5p	Whsc1l1	mmu-miR-199a-3p	Smad1	mmu-miR-297a-5p	Zfp748
mmu-miR-17-5p	Dync1li2	mmu-miR-199a-3p	Cox-2	mmu-miR-297a-5p	Mfsd4
mmu-miR-17-5p	Med17	mmu-miR-199a-3p	COX2	mmu-miR-297a-5p	Zfp521
mmu-miR-17-5p	Scn3b	mmu-miR-199a-3p	Runx1	mmu-miR-297a-5p	Vezt
mmu-miR-17-5p	Usp3	mmu-miR-199b-3p	Dyrk1a	mmu-miR-297a-5p	Eea1
mmu-miR-17-5p	Fam63b	mmu-miR-1a-3p	Anxa5	mmu-miR-297a-5p	Glce
mmu-miR-17-5p	Arhgef9	mmu-miR-1a-3p	Srf	mmu-miR-297a-5p	15-Sep
mmu-miR-17-5p	Lrp11	mmu-miR-1a-3p	Tlx2	mmu-miR-297a-5p	Csnk1a1
mmu-miR-17-5p	Lrrc3	mmu-miR-1a-3p	Myh6	mmu-miR-297a-5p	Mpv17l
mmu-miR-17-5p	C2cd4c	mmu-miR-1a-3p	Rheb	mmu-miR-297a-5p	Aff4
mmu-miR-17-5p	Gpatch8	mmu-miR-1a-3p	Calm2	mmu-miR-297a-5p	Nipa2
mmu-miR-17-5p	Zfp367	mmu-miR-1a-3p	Ucp2	mmu-miR-297a-5p	Brwd1
mmu-miR-17-5p	Cadm2	mmu-miR-1a-3p	Fn1	mmu-miR-297a-5p	Slc4a10
mmu-miR-17-5p	Tor1aip2	mmu-miR-1a-3p	Rps6	mmu-miR-297a-5p	Wwtr1
mmu-miR-17-5p	Lrrc55	mmu-miR-1a-3p	Irx5	mmu-miR-297a-5p	Map4k3
mmu-miR-17-5p	Slc7a14	mmu-miR-1a-3p	Pola1	mmu-miR-297a-5p	2700081O15Rik
mmu-miR-17-5p	Slc44a5	mmu-miR-1a-3p	Acta1	mmu-miR-297a-5p	Synj1
mmu-miR-17-5p	Gabbr2	mmu-miR-1a-3p	Calm1	mmu-miR-297a-5p	Acly
mmu-miR-17-5p	Rundc3b	mmu-miR-1a-3p	Klf4	mmu-miR-297a-5p	Smek2
mmu-miR-17-5p	Kbtbd8	mmu-miR-1a-3p	Cdc42	mmu-miR-297a-5p	Iars
mmu-miR-17-5p	Rgma	mmu-miR-1a-3p	Cdk9	mmu-miR-297a-5p	Dusp22
mmu-miR-17-5p	Zfp317	mmu-miR-1a-3p	Gata4	mmu-miR-297a-5p	Ankrd28
mmu-miR-17-5p	Npat	mmu-miR-1a-3p	Igf1r	mmu-miR-297a-5p	Sharpin
mmu-miR-17-5p	Tbc1d8b	mmu-miR-1a-3p	Gja1	mmu-miR-297a-5p	Srl
mmu-miR-17-5p	Fat2	mmu-miR-1a-3p	Pax7	mmu-miR-297a-5p	Ppm1l
mmu-miR-17-5p	Alkbh5	mmu-miR-1a-3p	Mef2a	mmu-miR-297a-5p	Ranbp3l
mmu-miR-17-5p	Rab11fip4	mmu-miR-1a-3p	Hand2	mmu-miR-297a-5p	Tm6sf1
mmu-miR-17-5p	Zfp652	mmu-miR-1a-3p	Rasa1	mmu-miR-297a-5p	Grm5
mmu-miR-17-5p	Rapgefl1	mmu-miR-1a-3p	Hspa1b	mmu-miR-297a-5p	Erc2
mmu-miR-17-5p	Lsamp	mmu-miR-1a-3p	Nppa	mmu-miR-297a-5p	Fam73b
mmu-miR-17-5p	Robo2	mmu-miR-1a-3p	Hdac4	mmu-miR-297a-5p	Tspan9
mmu-miR-17-5p	Nrip1	mmu-miR-1a-3p	Igf1	mmu-miR-297a-5p	Prex2
mmu-miR-17-5p	Ppp2r2c	mmu-miR-1a-3p	Hspd1	mmu-miR-297a-5p	Zbtb34
mmu-miR-17-5p	Ogfod1	mmu-miR-203-3p	Zfp281	mmu-miR-297a-5p	Slc6a7
mmu-miR-17-5p	Flnb	mmu-miR-203-3p	Trp63	mmu-miR-297a-5p	Cdh7
mmu-miR-17-5p	Casc4	mmu-miR-205-5p	Lrrk2	mmu-miR-297a-5p	Gpr158
mmu-miR-17-5p	Islr2	mmu-miR-205-5p	Pten	mmu-miR-297a-5p	Zfp160
mmu-miR-17-5p	Zhx3	mmu-miR-27a-3p	Odc1	mmu-miR-297a-5p	Camta2
mmu-miR-17-5p	Itgb8	mmu-miR-27a-3p	Runx1	mmu-miR-297a-5p	Taok1
mmu-miR-17-5p	Ep300	mmu-miR-27a-3p	Srm	mmu-miR-297a-5p	Pak2
mmu-miR-17-5p	D630045J12Rik	mmu-miR-27a-3p	Pparg	mmu-miR-297a-5p	Suco
mmu-miR-17-5p	Tmcc1	mmu-miR-297a-5p	Stk3	mmu-miR-297a-5p	Mtmr6
mmu-miR-17-5p	Frmpd4	mmu-miR-297a-5p	Kcnab1	mmu-miR-297a-5p	Slc39a10
mmu-miR-17-5p	Nr1d2	mmu-miR-297a-5p	Kcnj3	mmu-miR-297a-5p	C030046E11Rik
mmu-miR-17-5p	Prune2	mmu-miR-297a-5p	Kcna1	mmu-miR-297a-5p	Fermt2
mmu-miR-17-5p	Pcdhac1	mmu-miR-297a-5p	Slc39a9	mmu-miR-297a-5p	Nxt2
mmu-miR-17-5p	Nefh	mmu-miR-297a-5p	Agfg1	mmu-miR-297a-5p	Tardbp
mmu-miR-17-5p	Lrch1	mmu-miR-297a-5p	Insr	mmu-miR-297a-5p	Larp4b
mmu-miR-17-5p	N4bp2l2	mmu-miR-297a-5p	Rxfp1	mmu-miR-297a-5p	Ago1
mmu-miR-17-5p	Taok2	mmu-miR-297a-5p	Zc3h12b	mmu-miR-297a-5p	Megf9
mmu-miR-17-5p	Tmed8	mmu-miR-297a-5p	Kcnc1	mmu-miR-297a-5p	Zfp217
mmu-miR-17-5p	Rnf213	mmu-miR-297a-5p	Kcnh1	mmu-miR-297a-5p	Amigo1
mmu-miR-17-5p	Ildr2	mmu-miR-297a-5p	Dnm3	mmu-miR-297a-5p	Lingo3
mmu-miR-17-5p	Slc7a2	mmu-miR-297a-5p	Tnks	mmu-miR-483-5p	Socs3
mmu-miR-17-5p	Bcl2l11	mmu-miR-297a-5p	Ketd21	mmu-miR-486-5p	Pten
mmu-miR-17-5p	Bmp4	mmu-miR-297a-5p	Tmcc1	mmu-miR-486-5p	Foxo1
mmu-miR-17-5p	Btg2	mmu-miR-297a-5p	Chsy1	mmu-miR-486-5p	Pax7
mmu-miR-17-5p	C1qa	mmu-miR-297a-5p	Rab9b		

Wnt signaling pathway was specifically regulated by the DEmiRs in the femur but not in the mandible (Fig. 6b). A total of five miRNAs (i.e., miR-125b-5p, -297a-5p, -17-5p, -199a-3p, and -133a-3p) were responsible for the regulation of the TGF-β signaling pathway in the mandible, and two miRNAs (i.e., miR-133a-3p and -133-5p) were involved in the regulation of the Wnt signaling pathway in the femur. The results of the quantitative real-time PCR also validated the DEmiRs in the mandible and femur in OVX (Fig. 7a, b).

Overall, these results suggest that miR-297a-5p, -17-5p, -133a-3p and 133-5p may have important roles in bone mass loss in the context of estrogen-deficiency states. The different expression tendencies of miR-17-5p and miR-133a-3p showed different functions between the miRNA in the mandible and in the femur.

Discussion

Estrogen deficiency can cause osteoporosis in different bone structures. Numerous studies have demonstrated the association between skeletal BMD and bone loss in the mandible [9, 33]. Some clinical studies have reported that the alveolar bone shows more resorption in osteoporotic versus non-osteoporotic edentulous patients [34, 35]. However, clinical analyses of the human jaw have not yet conclusively demonstrated that estrogen deficiency can cause bone loss in human jaw bones [36, 37]. These inconsistent results may be due to the heterogeneity among these studies; for example, the investigators use different techniques to measure skeletal and mandibular BMD and are interested in different anatomical sites. In addition, jawbones display very different anatomical characteristics from other bones of the skeleton. The presence of teeth leads to the difference that is distinguished as the "basal bone" and the tooth-bearing "alveolar process." Individual variation arising from the number of tooth loss and the severity of the periodontitis may also make it more complicated to analyze the mandible in postmenopausal women. Animal models are needed to investigate the changes induced by estrogen deficiency in the mandible. In our animal model, we found that the trabecular bone of the distal femur and alveolar bone are significantly decreased three months after OVX. However, the BV/TV of the mandible decreases less than that of the distal femur in the OVX group. The tooth is not extracted from the mandible; hence, the mechanical loading of the alveolar bone during mastication may alleviate bone loss induced by estrogen deficiency. Our animal models consist of dentulous patients suffering from estrogen deficiency. More studies are needed to explore the combined effect of tooth loss and estrogen deficiency on mandibular bone loss in the future.

Table 5. The 27 validated miRNA-target pairs, including 22 genes and 5 DEmiRs in femur

miRNA	Target gene
mmu-miR-127	Rtl1/Peg11
mmu-miR-133a	Runx2
mmu-miR-133a	Cdc42
mmu-miR-133a	Whsc2
mmu-miR-133a	RhoA
mmu-miR-133a	SRF
mmu-miR-133a-3p	Hdac4
mmu-miR-133a-3p	Cdc42
mmu-miR-133a-3p	Casp9
mmu-miR-133a-3p	Rhoa
mmu-miR-133a-3p	Srf
mmu-miR-133a-3p	Igf1r
mmu-miR-133a-3p	Runx2
mmu-miR-133a-3p	Ccnd2
mmu-miR-133a-3p	Nfatc4
mmu-miR-133a-3p	Ucp2
mmu-miR-133a-3p	Spry1
mmu-miR-133a-3p	Pola1
mmu-miR-133a-3p	Nelfa
mmu-miR-136	Rtl1/Peg11
mmu-miR-206	Pola1
mmu-miR-206	B-ind1
mmu-miR-206	Gja1
mmu-miR-206	Fstl1
mmu-miR-206	Utrn
mmu-miR-206	Cx43
mmu-miR-206	Mmd

Aside from the anatomical/physiological peculiarities of the mandible, its metabolism response may also differ from that of the skeletal bone. MiRNA may have its own roles in regulating metabolism response induced by estrogen deficiency. In this study, we screened DEmiRs and identified the key miRNAs involved in the regulation of mandibular osteoporosis. The estrogen deficiency mice model was successfully established using mice that underwent OVX. BMD was decreased in both the femur and mandible of mice after OVX. The result of miRNA array analysis showed 53 DEmiRs in the mandible of the OVX and sham-operated mice. Through miRNA-mRNA regulation network analysis, we identified that 15 out of the 53 DEmiRs may have a pivotal role in the network, given that these DEmiRs are significantly involved in the regulation of 33 biological pathways, such as the MAPK signaling pathway, pathways in cancer, axon guidance, glioma, and TGF-β signaling pathway.

Among the 15 DEmiRs, 6 miRNA (i.e., miR-297a-5p, -483-5p, -133a-3p, -133b-3p, -1a-3p, and -486-5p) were identified to be down-regulated in the mandible of OVX mice, and 9 miRNA (i.e., miR-203p-3p, -125b-5p, -15b-5p, -17-5p, -27a-3p, -199a-3p, -199b-3p,

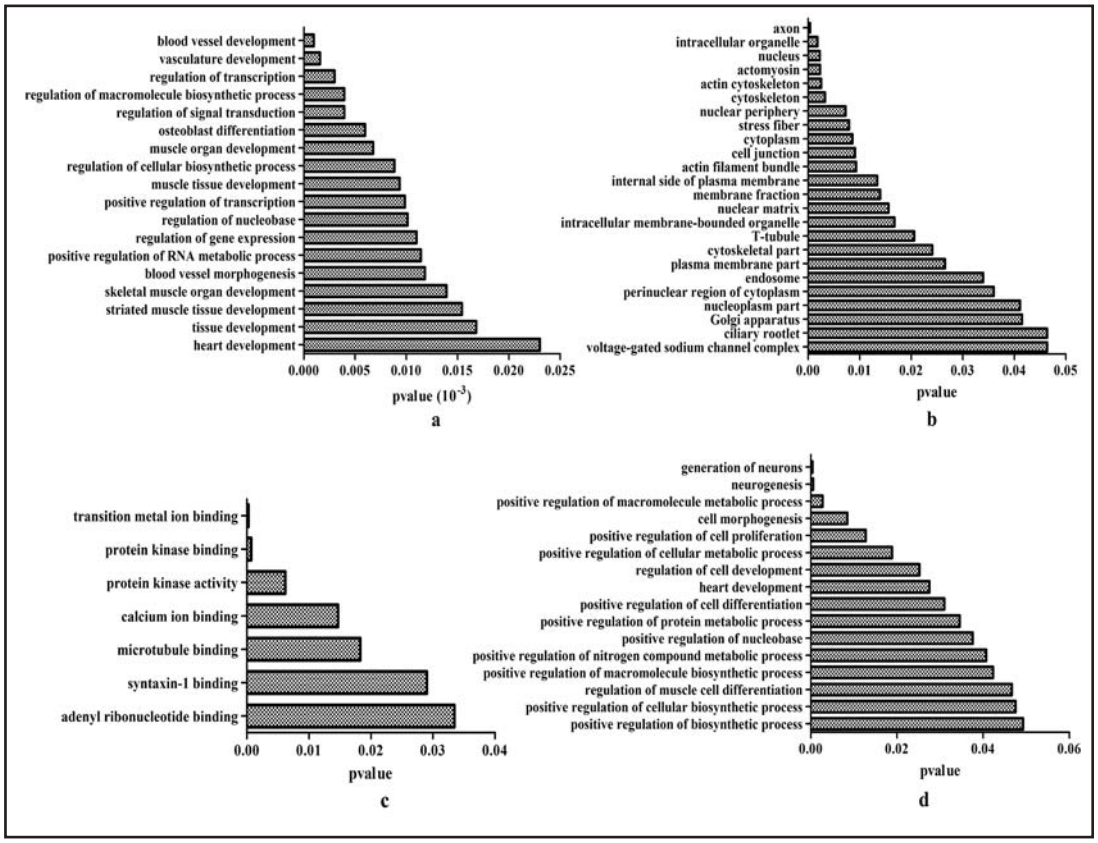

Fig. 4. Function enrichment analysis of the validated target genes of the DEmiRs in the mandible and femur. Function enrichment analysis of the 666 validated target genes of the 15 DEmiRs. Three aspects of gene ontology were analyzed: (a) biological process, (b) cellular component, (c) molecular function, and (d) function enrichment analysis of the validated target genes of miRNA in the femur of OVX mice (i.e., data extracted from An et al. [26]) The 22 target genes of the 5 DEmiRs were used for function enrichment analysis. This figure shows the results of mixed gene ontology analysis of the function analysis.

-125a-5p, and -205-5p) were up-regulated compared with the sham-operated mice. These results were validated by quantitative real-time PCR (Fig. 7). Some have been reported to be involved in bone metabolism. For example, miR-1 significantly induces chondrocyte proliferation and differentiation via the direct targeting of histone deacetylase 4 (HDAC4) [38]. MiR-27a-3p is down-regulated in murine bone marrow stromal cells, in which Satb2 is overexpressed to induce osteogenic differentiation [39]. The suppression of miR-203 improves the survival of rat bone marrow mesenchymal stem cells by enhancing PI3K-induced cellular activation [40]. Given the fact that BMD is significantly decreased by OVX in our study, the results significantly increase the expression of miR-27a-3p and miR-203-3p and decrease miR-1a-3p, which influences proliferation, and the differentiation of the bone cells are consistent with previous studies. In addition, miR-125b-5p, which has been reported to inhibit the osteoblastic differentiation [41] and osteogenic differentiation of human bone marrow mesenchymal stem cells [42], displays upregulation in osteoporotic patients [43]. miR-125a-5p, which is from the same family as miR-125b-5p, also has a negative role in the osteogenic differentiation of bone marrow stromal cells [44] and adipose-derived stem cells [45]. In our study, the expression of miR-125b-5p and miR-125a-5p are both up-regulated in the mandible of OVX mice compared with sham-operated mice. The negative role of miR-125b-5p and miR-125a-5p in osteogenic differentiation may significantly affect the osteogenic differentiation of bone marrow stromal cells in the mandible of OVX mice [46], which inhibits bone formation [47].

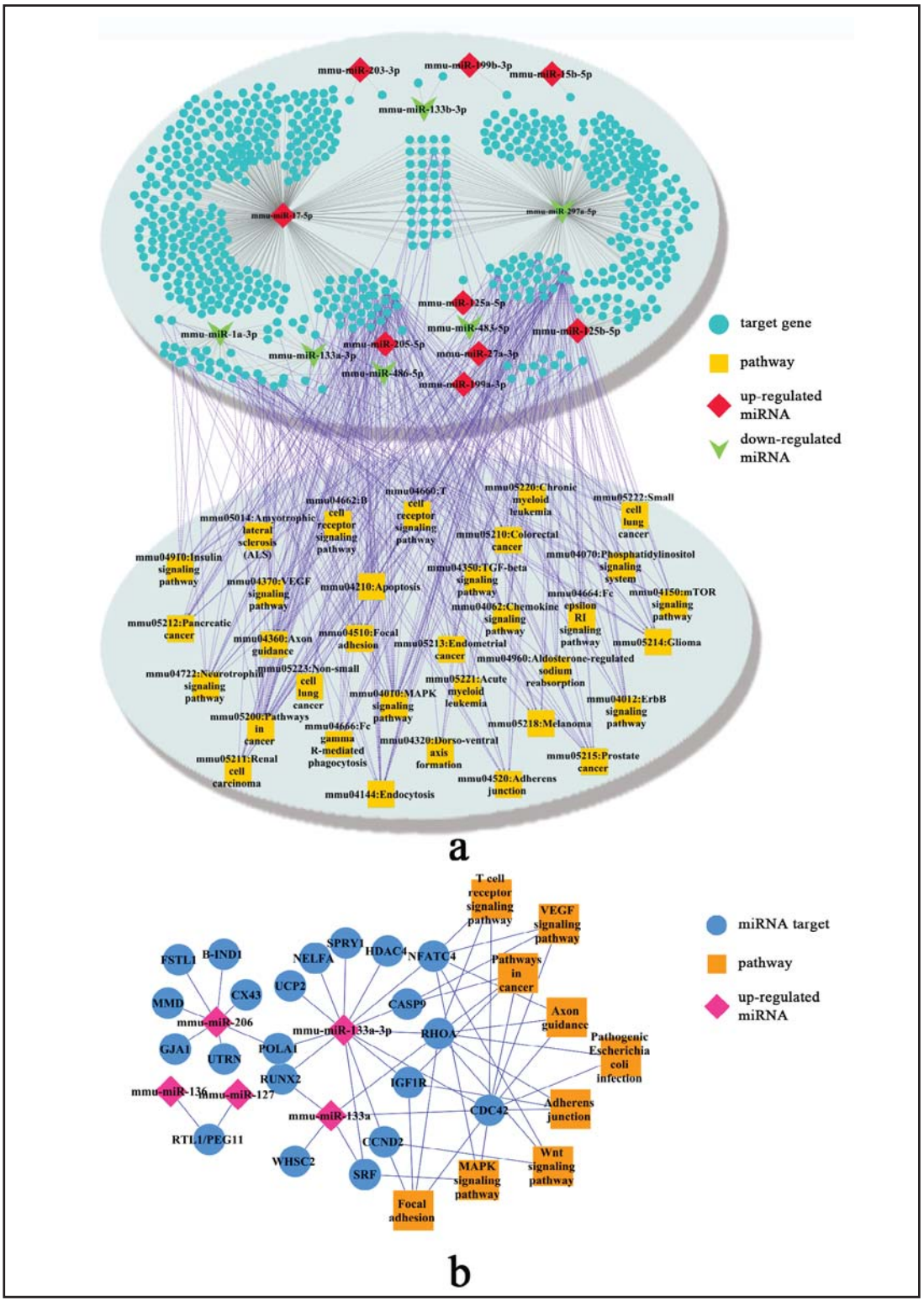

Fig. 5. miRNA-mRNA-pathway complex network in the mandible and femur of OVX mice. (a) The miRNA-mRNA interaction network, which consists of DEmiRs and their experimentally validated miRNA-target genes. The significant pathways are connected to this network based on the KEGG database. (b) The miRNA-mRNA-pathway complex network in the femurs of OVX mice (i.e., data extracted from An et al. [26]). The miRNA-mRNA-pathway complex network, which consists of five DEmiRs and their experimentally validated miRNA-target genes.

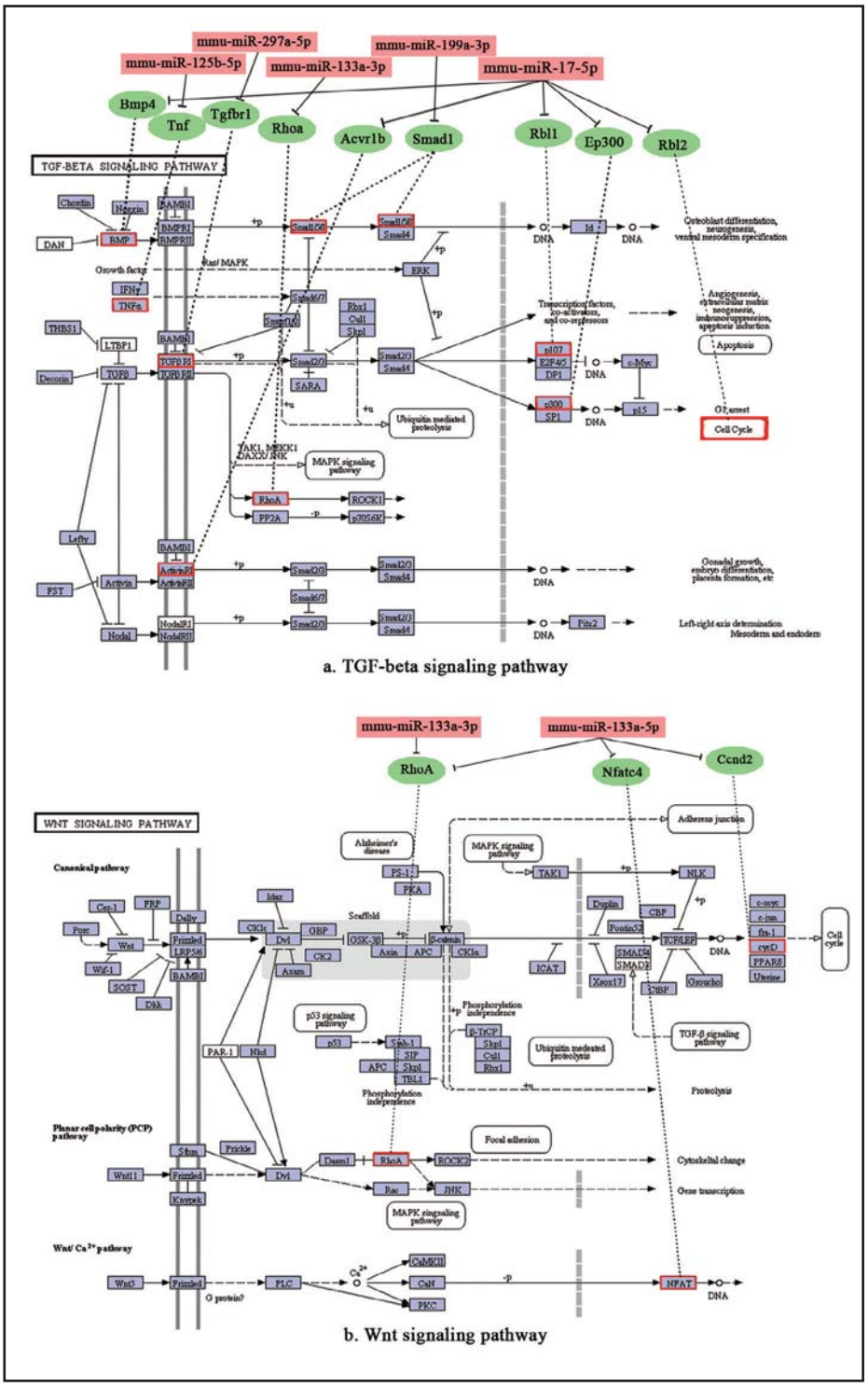

Fig. 6. Specifical pathways in mandible and femur. When the different regulation pathways of DEmiRs in the mandible and femur were compared after OVX, the different ways of regulation were obtained: (a) the TGF-β signaling pathway in the mandible of OVX mice and (b) the Wnt signaling pathway in the femur of OVX mice.

An et al. showed that the expression of miR-133b-3p and miR-133a-3p are significantly up-regulated in the femur of OVX mice [26] and are significantly down-regulated in the mandible of OVX mice in our study. The study conducted by Li et al. also showed that the expression of miR-133a-3p is down-regulated during bone morphogenetic protein 2 (BMP2)-induced osteogenesis in C2C12 mesenchymal cells [48]. However, some studies have reported that the mandibular alveolar bone is less sensitive to OVX than the long bone [16, 17]. The down-regulated miR-133a-3p in the mandible of OVX mice may have

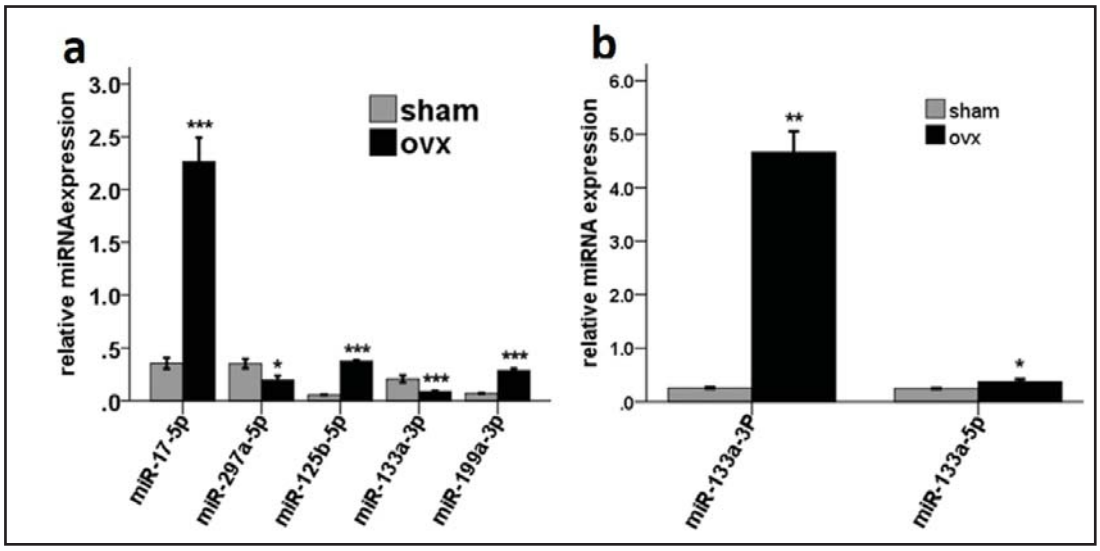

Fig. 7. Results of the quantitative real-time PCR validated the DEmiRs in the mandible and femur in OVX. (a) The real-time-PCR results of DEmiRs in the mandible. (b) The realtime-PCR results of DEmiRs in the femur * $p < 0.05$,** $p < 0.01$,*** $p < 0.001$.

a protective effect on the bone loss of the mandible. This may be one of the reasons why bone loss in the mandible is milder than that in the long bones of OVX animals. Moreover, several other DEmiRs are not found in the femur in our study. The mandible is a special tissue developed from the neuroectoderm and constantly undergoes mechanical stress, such as occlusal pressure. Essentially, osteoporosis is hypothesized as a risk factor for tooth loss in postmenopausal women [49, 50], and vice versa. Previous reports indicated that tooth loss early in life impairs the dynamic homeostasis of bone formation and bone resorption by activating a stress hormone, corticosterone, leading to reduced bone strength in mice with age [51, 52]. The toothless mice show a decrease in the trabecular bone volume fraction of the vertebra and femur with age. Thus, long-term tooth loss may have accumulative negative effect on bone health, accelerating bone loss [52]. By contrast, a higher number of remaining teeth is found to be associated with higher BMD in postmenopausal women [53]. Furthermore, some dental tissue-related signalings, such as the transcription factors Msx1, Twist, and Snail, which are the downstream targets of FGF and BMP signaling relevant to tooth development and bone remodeling, may also contribute to the difference between the mandible and femur [54, 55]. The local environment and metabolic mechanism of the alveolar bone markedly differs from those of other bones [48]. The mandible and femur are morphologically and functionally different from each other, as well as the miRNAs and its mechanism involved in the regulation of bone remolding.

In addition, we analyzed the miRNA-mRNA-pathway complex network in the mandible and femur of OVX mice using the online tool DAVID. Function comparison analysis showed that the different expressed miRNAs regulated the following pathways both in the mandible and femur after OVX: focal adhesion, VEGF signaling pathway, adherens junction, T-cell receptor signaling pathway, pathways in cancer, axon guidance, and MAPK signaling pathway.

Interestingly, we found that the TGF-β signaling pathway and WNT signaling pathway are significant and specifical pathways involved in the regulation of mandible and femur, respectively. Specifically, the DEmiRs of the mandible uniquely regulate the mTOR signaling pathway, ErbB signaling pathway, Fc gamma R-mediated phagocytosis, TGF-β signaling pathway, Jak-STAT signaling pathway, and chronic and acute myeloid leukemia. In these pathways, the TGF-β signaling pathway is critical to cell lineage determination during endochondral ossification as a positive regulator for chondrocytes [56]and a negative

regulator for osteoblasts [57-59]. In the mandible of OVX mice, five miRNAs (i.e., miR-17-5p, miR-133a-3p, miR-125b-5p, miR-199a-3p, and miR-297a-5p) are significantly involved in regulating the TGF-β signaling pathway. TGF-β, a secreted factor, has a key role in proliferation and differentiation during skeletogenesis. In the TGF-β signaling pathway, miR-297a-5p targets Tgfbr1 (i.e., the transforming growth factor β receptor1), which is a critical regulator of tissue repair. A disrupted TGF-β1 signaling pathway is associated with delayed periodontal repair and further induces the bisphosphonate-associated osteonecrosis of the mandible [60]. BMP2, a multifunctional growth factor that belongs to the TGF-β superfamily, is involved in the regulation of the proliferation, differentiation, migration, and apoptosis of various cell types [61]. Moreover, BMP2 is well known to have an essential role in bone formation, including tooth development, especially in regulating osteoblastic differentiation, which has a key role in bone remodeling. BMP2 can also help bone regeneration and repair and prevent apoptosis [62]. Recent research has demonstrated that BMP2 can promote mesenchymal cell conversion to osteoblasts [63]. BMP2 and BMP4 appear to accelerate alveolar bone development [64]. Many preclinical and clinical studies support utilizing BMP2 in therapeutic interventions, such as bone defects and osteoporosis [65]. BMP2 is the target of miR-17-5p [66]. In our study, miR-17-5p is up-regulated in the mandible after OVX, and it further inhibits the TGF-β signaling pathway in the mandible of OVX mice. miR-17-5p regulates the bone morphogenetic protein signaling pathway by repressing the expression of the bone morphogenetic protein type II receptor [67]. Moreover, the upregulation of miR-17-5p suppresses osteogenesis and increases adipogenesis [67, 68]. Therefore, we suggest that the TGF-β signaling pathway is significantly correlated with the development of the mandible.

Compared with those in the mandible, the DEmiRs in the femur after OVX are specifically involved in the Wnt signaling pathway. The Wnt signaling pathway has a key role in the regulation of long bone growth and turnover [69] and development of osteoporosis [70]. In the femur of the OVX mice, miR-133a-3p and miR-133a-5p are significantly associated with the regulation of the Wnt signaling pathway. Both miR-133a-5p and miR-133a-3p are significantly up-regulated in the femur of OVX mice compared with those in the sham-operated group. Moreover, the upregulation of miR-133a is validated in the plasma of osteoporosis and osteopenia patients versus the normal group [71, 72]. Thus, the Wnt signaling pathway is specifically regulated by the miR-133a-3p and -133a-5p in the femur.

The TGF-β signaling and Wnt signaling pathways have a close relationship, both of which have an important role in regulating embryonic development, fibrotic disease, and tumor progression. Studies have found several typical cross points between these two signaling systems, such as Smad, Axin, Dvl, and β-catenin. Our study found that RHOA affects both the TGF-β signaling pathway and Wnt signaling pathway. MiR-133a-3p is down-regulated in the mandible of OVX mice, and it promotes the RHOA and further activates the TGF-β signaling pathway. In the femur of OVX mice, the miR-133a-3p is up-regulated and further inhibits the Wnt signaling pathway. The different expression tendencies of miR-133a-3p likely induce the tissue-specificity between the mandible and femur.

The results of the miRNA-mRNA interaction anaylsis suggest that miR-17-5p and miR-297a-5p are the hubs of the miRNA-mRNA network. In addition, they significantly influence the biological pathways. miR-17-5p is up-regulated in our study, whereas miR-297a-5p is down-regulated. According to the previous study, the miR-297a-5p-targeted Tgfbr1 gene and miR-17-5p-targetd BMP4 gene are involved in bone metabolism. Thus, we propose that miR-17-5p and miR-297a-5p be considered potential biomarkers in the development of the mandible of OVX mice.

Conclusion

In summary, our study provides new insights into the role of miRNA in the regulation of osteoporosis of the mandible and femur. We obtain different ways of regulating estrogen

deficiency-induced osteoporosis in the mandible and femur by comparing miRNA expression data from these different bone sites. miR-17-5p and miR-133a-3p are identified as potential important biomarkers in the development of the mandible and femur. Their different expression tendencies indicate their special function in different tissues, and more experiments are needed to confirm the different functions of the mandible and femur after OVX.

Acknowledgments

This work was supported by the National Natural Science Foundation of China (Grant no. 81470716) and Science and Technology Committee Foundation of Shanghai (Grant no. 14411967200).

Disclosure Statement

All the authors have no conflict of interest.

References

1 Khosla S, Oursler MJ, Monroe DG: Estrogen and the skeleton. Trends Endocrinol Metab 2012;23:576-581.
2 Nicopoulou-Karayianni K, Tzoutzoukos P, Mitsea A, Karayiannis A, Tsiklakis K, Jacobs R, Lindh C, Van Der Stelt P, Allen P, Graham J, Horner K, Devlin H, Pavitt S, Yuan J: Tooth loss and osteoporosis: the OSTEODENT Study. J Clin Periodontol 2009;36:190-197.
3 Gur A, Nas K, Kayhan O, Atay MB, Akyuz G, Sindal D, Aksit R, Oncel S, Dilsen G, Cevik R, Gunduz OH, Ersoy Y, Altay Z, Ozturk C, Akkus S, Senocak O, Kavuncu V, Kirnap M, Tekeoglu I, Erdogan F, Sarac AJ, Demiralp L, Demirkesen A, Adam M: The relation between tooth loss and bone mass in postmenopausal osteoporotic women in Turkey: a multicenter study. J Bone Miner Metab 2003;21:43-47.
4 Bhatnagar S, Krishnamurthy V, Pagare SS: Diagnostic efficacy of panoramic radiography in detection of osteoporosis in post-menopausal women with low bone mineral density. J Clin Imaging Sci 2013;3:23-31.
5 Aguilera-Barreiro De LA, Davalos-Vazquez KF, Jimenez-Mendez C, Jimenez-Mendoza D, Olivarez-Padron LA, Rodriguez-Garcia ME: The relationship of nutritional status, body and mandibular bone mineral density, tooth loss and fracture risk (FRAX) in pre-and postmenopausal women with periodontitis. Nutr Hosp 2014;29:1419-1426.
6 Nackaerts O, Jacobs R, Devlin H, Pavitt S, Bleyen E, Yan B, Borghs H, Lindh C, Karayianni K, Van Der Stelt P, Marjanovic E, Adams JE, Horner K: Osteoporosis detection using intraoral densitometry. Dentomaxillofac Radiol 2008;37:282-287.
7 Shen EC, Gau CH, Hsieh YD, Chang CY, Fu E: Periodontal status in post-menopausal osteoporosis: a preliminary clinical study in Taiwanese women. J Chin Med Assoc 2004;67:389-393.
8 Guiglia R, Di Fede O, Lo Russo L, Sprini D, Rini GB, Campisi G: Osteoporosis, jawbones and periodontal disease. Med Oral Patol Oral Cir Bucal 2013;18:e93-99.
9 Barngkgei I, Al Haffar I, Khattab R: Osteoporosis prediction from the mandible using cone-beam computed tomography. Imaging Sci Dent 2014;44:263-271.
10 Anbinder AL, Prado Fde A, Prado Mde A, Balducci I, Rocha RF: The influence of ovariectomy, simvastatin and sodium alendronate on alveolar bone in rats. Braz Oral Res 2007;21:247-252.
11 Rawlinson SC, Boyde A, Davis GR, Howell PG, Hughes FJ, Kingsmill VJ: Ovariectomy vs. hypofunction: their effects on rat mandibular bone. J Dent Res 2009;88:615-620.
12 Zhang Y, Wei L, Miron RJ, Zhang Q, Bian Z: Prevention of alveolar bone loss in an osteoporotic animal model via interference of semaphorin 4d. J Dent Res 2014;93:1095-1100.
13 Zhang Z, Xiang L, Bai D, Wang W, Li Y, Pan J, Liu H, Wang S, Xiao G, Ju D: The Protective Effect of Rhizoma Dioscoreae Extract against Alveolar Bone Loss in Ovariectomized Rats via Regulating Wnt and p38 MAPK Signaling. Nutrients 2014;6:5853-5870.

14 Moriya Y, Ito K, Murai S: Effects of experimental osteoporosis on alveolar bone loss in rats. J Oral Sci 1998;40:171-175.
15 Kuroda S, Mukohyama H, Kondo H, Aoki K, Ohya K, Ohyama T, Kasugai S: Bone mineral density of the mandible in ovariectomized rats: analyses using dual energy X-ray absorptiometry and peripheral quantitative computed tomography. Oral Dis 2003;9:24-28.
16 Mavropoulos A, Rizzoli R, Ammann P: Different responsiveness of alveolar and tibial bone to bone loss stimuli. J Bone Miner Res 2007;22:403-410.
17 Zhang Y, Li Y, Gao Q, Shao B, Xiao J, Zhou H, Niu Q, Shen M, Liu B, Hu K, Kong L: The variation of cancellous bones at lumbar vertebra, femoral neck, mandibular angle and rib in ovariectomized sheep. Arch Oral Biol 2014;59:663-669.
18 Elovic RP, Hipp JA, Hayes WC: Ovariectomy decreases the bone area fraction of the rat mandible. Calcif Tissue Int 1995;56:305-310.
19 Li H, Xie H, Liu W, Hu R, Huang B, Tan YF, Xu K, Sheng ZF, Zhou HD, Wu XP, Luo XH: A novel microRNA targeting HDAC5 regulates osteoblast differentiation in mice and contributes to primary osteoporosis in humans. J Clin Invest 2009;119:3666-3677.
20 Bae Y, Yang T, Zeng HC, Campeau PM, Chen Y, Bertin T, Dawson BC, Munivez E, Tao J, Lee BH: miRNA-34c regulates Notch signaling during bone development. Hum Mol Genet 2012;21:2991-3000.
21 Yang N, Wang G, Hu C, Shi Y, Liao L, Shi S, Cai Y, Cheng S, Wang X, Liu Y, Tang L, Ding Y, Jin Y: Tumor necrosis factor alpha suppresses the mesenchymal stem cell osteogenesis promoter miR-21 in estrogen deficiency-induced osteoporosis. J Bone Miner Res 2013;28:559-573.
22 Liao L, Yang X, Su X, Hu C, Zhu X, Yang N, Chen X, Shi S, Shi S, Jin Y: Redundant miR-3077-5p and miR-705 mediate the shift of mesenchymal stem cell lineage commitment to adipocyte in osteoporosis bone marrow. Cell Death Dis 2013;4:e600-613.
23 Wang X, Guo B, Li Q, Peng J, Yang Z, Wang A, Li D, Hou Z, Lv K, Kan G, Cao H, Wu H, Song J, Pan X, Sun Q, Ling S, Li Y, Zhu M, Zhang P, Peng S, Xie X, Tang T, Hong A, Bian Z, Bai Y, Lu A, Li Y, He F, Zhang G, Li Y: miR-214 targets ATF4 to inhibit bone formation. Nat Med 2013;19:93-100.
24 Zhang Y, Su J, Teng Y, Zhang J, Wang J, Li K, Yao L, Li X: Nrp1, a Neuronal Regulator, Enhances DDR2-ERK-Runx2 Cascade in Osteoblast Differentiation via Suppression of DDR2 Degradation. Cell Physiol Biochem 2015;36:75-84.
25 Liu XD, Cai F, Liu L, Zhang Y, Yang AL: MicroRNA-210 is involved in the regulation of postmenopausal osteoporosis through promotion of VEGF expression and osteoblast differentiation. Biol Chem 2015;396:339-347.
26 An JH, Ohn JH, Song JA, Yang JY, Park H, Choi HJ, Kim SW, Kim SY, Park WY, Shin CS: Changes of microRNA profile and microRNA-mRNA regulatory network in bones of ovariectomized mice. J Bone Miner Res 2014;29:644-656.
27 Zhang Z, Song C, Zhang F, Xiang L, Chen Y, Li Y, Pan J, Liu H, Xiao GG, Ju D: Rhizoma Dioscoreae extract protects against alveolar bone loss in ovariectomized rats via microRNAs regulation. Nutrients 2015;7:1333-1351.
28 Sethupathy P, Corda B, Hatzigeorgiou AG: TarBase: A comprehensive database of experimentally supported animal microRNA targets. RNA 2006;12:192-197.
29 Hsu SD, Lin FM, Wu WY, Liang C, Huang WC, Chan WL, Tsai WT, Chen GZ, Lee CJ, Chiu CM, Chien CH, Wu MC, Huang CY, Tsou AP, Huang HD: miRTarBase: a database curates experimentally validated microRNA-target interactions. Nucleic Acids Res 2011;39:D163-169.
30 Xiao F, Zuo Z, Cai G, Kang S, Gao X, Li T: miRecords: an integrated resource for microRNA-target interactions. Nucleic Acids Res 2009;37:D105-110.
31 Huang Da W, Sherman BT, Lempicki RA: Systematic and integrative analysis of large gene lists using DAVID bioinformatics resources. Nat Protoc 2009;4:44-57.
32 Li Z, Wang J, Wang Y, Jiang H, Xu X, Zhang C, Li D, Xu C, Zhang K, Qi Y, Gong X, Tang C, Zhong N, Lu W: Bone morphogenetic protein 4 inhibits liposaccharide-induced inflammation in the airway. Eur J Immunol 2014;44:3283-3294.
33 Rehman DE, Sarwath S, Nigar S: Association between changes in the angle of mandible and reduced bone mineral density. J Coll Physicians Surg Pak 2015;25:87-90.
34 Hirai T, Ishijima T, Hashikawa Y, Yajima T: Osteoporosis and reduction of residual ridge in edentulous patients. J Prosthet Dent 1993;69:49-56.

35 Singhal S, Chand P, Singh BP, Singh SV, Rao J, Shankar R, Kumar S: The effect of osteoporosis on residual ridge resorption and masticatory performance in denture wearers. Gerodontology 2012; 29: e1059-1066.
36 Ozola B, Slaidina A, Laurina L, Soboleva U, Lejnieks A: The influence of bone mineral density and body mass index on resorption of edentulous jaws. Stomatologija 2011;13:19-24.
37 Springe B, Slaidina A, Soboleva U, Lejnieks A: Bone mineral density and mandibular residual ridge resorption. Int J Prosthodont 2014;27:270-276.
38 Li P, Wei X, Guan Y, Chen Q, Zhao T, Sun C, Wei L: MicroRNA-1 regulates chondrocyte phenotype by repressing histone deacetylase 4 during growth plate development. Faseb J 2014;28:3930-3941.
39 Gong Y, Xu F, Zhang L, Qian Y, Chen J, Huang H, Yu Y: MicroRNA expression signature for Satb2-induced osteogenic differentiation in bone marrow stromal cells. Mol Cell Biochem 2014;387:227-239.
40 Liu T, Fu NN, Song HL, Wang YL, Wu BJ, Shen ZY: Suppression of MicroRNA-203 improves survival of rat bone marrow mesenchymal stem cells through enhancing PI3K-induced cellular activation. IUBMB Life 2014:220-227. doi: 10.1002/iub.1259.
41 Mizuno Y, Yagi K, Tokuzawa Y, Kanesaki-Yatsuka Y, Suda T, Katagiri T, Fukuda T, Maruyama M, Okuda A, Amemiya T, Kondoh Y, Tashiro H, Okazaki Y: miR-125b inhibits osteoblastic differentiation by down-regulation of cell proliferation. Biochem Biophys Res Commun 2008;368:267-272.
42 Lu X, Deng M, He H, Zeng D, Zhang W: miR-125b regulates osteogenic differentiation of human bone marrow mesenchymal stem cells by targeting Smad4. Zhong Nan Da Xue Xue Bao Yi Xue Ban 2013;38:341-346.
43 Seeliger C, Karpinski K, Haug AT, Vester H, Schmitt A, Bauer JS, Van Griensven M: Five freely circulating miRNAs and bone tissue miRNAs are associated with osteoporotic fractures. J Bone Miner Res 2014;29:1718-1728.
44 Gong YM, Xu F, Zhang L, Qian YY, Chen JK, Huang HJ, Yu YC: MicroRNA expression signature for Satb2-induced osteogenic differentiation in bone marrow stromal cells. Mol Cell Biochem 2014;387:227-239.
45 Zhang ZJ, Zhang H, Kang Y, Sheng PY, Ma YC, Yang ZB, Zhang ZQ, Fu M, He AS, Liao WM: miRNA expression profile during osteogenic differentiation of human adipose-derived stem cells. J Cell Biochem 2012;113:888-898.
46 Xiao WL, Zhang DZ, Fan CH, Yu BJ: Intermittent Stretching and Osteogenic Differentiation of Bone Marrow Derived Mesenchymal Stem Cells via the p38MAPK-Osterix Signaling Pathway. Cell Physiol Biochem 2015;36:1015-1025.
47 Jiang T, Zhou B, Huang L, Wu H, Huang J, Liang T, Liu H, Zheng L, Zhao J: Andrographolide Exerts Pro-Osteogenic Effect by Activation of Wnt/beta-Catenin Signaling Pathway *in Vitro*. Cell Physiol Biochem 2015;36:2327-2339.
48 Li Z, Hassan MQ, Volinia S, Van Wijnen AJ, Stein JL, Croce CM, Lian JB, Stein GS: A microRNA signature for a BMP2-induced osteoblast lineage commitment program. Proc Natl Acad Sci USA 2008;105:13906-13911.
49 Numoto Y, Mori T, Maeda S, Tomoyasu Y, Higuchi H, Egusa M, Miyawaki T: Low bone mass is a risk factor in periodontal disease-related tooth loss in patients with intellectual disability. Open Dent J 2013;7:157-161.
50 Darcey J, Horner K, Walsh T, Southern H, Marjanovic EJ, Devlin H: Tooth loss and osteoporosis: to assess the association between osteoporosis status and tooth number. Br Dent J 2013;214:E10-19.
51 Furuzawa M, Chen H, Fujiwara S, Yamada K, Kubo KY: Chewing ameliorates chronic mild stress-induced bone loss in senescence-accelerated mouse (SAMP8), a murine model of senile osteoporosis. Exp Gerontol 2014;55:12-18.
52 Kurahashi M, Kondo H, Iinuma M, Tamura Y, Chen H, Kubo KY: Tooth loss early in life accelerates age-related bone deterioration in mice. Tohoku J Exp Med 2015;235:29-37.
53 Jang KM, Cho KH, Lee SH, Han SB, Han KD, Kim YH: Tooth loss and bone mineral density in postmenopausal South Korean women: The 2008-2010 Korea National Health and Nutrition Examination Survey. Maturitas 2015;82:360-364.
54 Meng T, Huang Y, Wang S, Zhang H, Dechow PC, Wang X, Qin C, Shi B, D'souza RN, Lu Y: Twist1 Is Essential for Tooth Morphogenesis and Odontoblast Differentiation. J Biol Chem 2015;290:29593-29602.
55 Rice R, Thesleff I, Rice DP: Regulation of Twist, Snail, and Id1 is conserved between the developing murine palate and tooth. Dev Dyn 2005;234:28-35.
56 Du G, Song Y, Wei L, Li L, Wang X, Xu Q, Zhan H, Cao Y, Zheng Y, Ding D: Osthole Inhibits Proliferation and Induces Catabolism in Rat Chondrocytes and Cartilage Tissue. Cell Physiol Biochem 2015;36:2480-2493.

57 Parada C, Li J, Iwata J, Suzuki A, Chai Y: CTGF mediates Smad-dependent transforming growth factor beta signaling to regulate mesenchymal cell proliferation during palate development. Mol Cell Biol 2013;33:3482-3493.
58 Oka K, Oka S, Hosokawa R, Bringas P, Jr., Brockhoff HC, 2nd, Nonaka K, Chai Y: TGF-beta mediated Dlx5 signaling plays a crucial role in osteo-chondroprogenitor cell lineage determination during mandible development. Dev Biol 2008;321:303-309.
59 Serra R, Chang C: TGF-beta signaling in human skeletal and patterning disorders. Birth Defects Res C Embryo Today 2003;69:333-351.
60 Wehrhan F, Hyckel P, Guentsch A, Nkenke E, Stockmann P, Schlegel KA, Neukam FW, Amann K: Bisphosphonate-associated osteonecrosis of the jaw is linked to suppressed TGFbeta1-signaling and increased Galectin-3 expression: a histological study on biopsies. J Transl Med 2011;9:102-112.
61 Wu J, Yu Z, Su D: BMP4 protects rat pulmonary arterial smooth muscle cells from apoptosis by PI3K/AKT/Smad1/5/8 signaling. Int J Mol Sci 2014;15:13738-13754.
62 Rosen V: BMP2 signaling in bone development and repair. Cytokine Growth Factor Rev 2009;20:475-480.
63 Farhadieh RD, Gianoutsos MP, Yu Y, Walsh WR: The role of bone morphogenetic proteins BMP-2 and BMP-4 and their related postreceptor signaling system (Smads) in distraction osteogenesis of the mandible. J Craniofac Surg 2004;15:714-718.
64 Ou M, Zhao Y, Zhang F, Huang X: Bmp2 and Bmp4 accelerate alveolar bone development. Connect Tissue Res 2015;56:204-211.
65 Ribeiro Filho SA, Francischone CE, De Oliveira JC, Ribeiro LZ, Do Prado FZ, Sotto-Maior BS: Bone augmentation of the atrophic anterior maxilla for dental implants using rhBMP-2 and titanium mesh: histological and tomographic analysis. Int J Oral Maxillofac Surg 2015;44:1492-1498.
66 Li H, Li T, Wang S, Wei J, Fan J, Li J, Han Q, Liao L, Shao C, Zhao RC: miR-17-5p and miR-106a are involved in the balance between osteogenic and adipogenic differentiation of adipose-derived mesenchymal stem cells. Stem Cell Res 2013;10:313-324.
67 Mao S, Li H, Sun Q, Zen K, Zhang CY, Li L: miR-17 regulates the proliferation and differentiation of the neural precursor cells during mouse corticogenesis. FEBS J 2014;281:1144-1158.
68 Tang L, Chen Y, Pei F, Zhang H: Lithium Chloride Modulates Adipogenesis and Osteogenesis of Human Bone Marrow-Derived Mesenchymal Stem Cells. Cell Physiol Biochem 2015;37:143-152.
69 Choi HY, Dieckmann M, Herz J, Niemeier A: Lrp4, a novel receptor for Dickkopf 1 and sclerostin, is expressed by osteoblasts and regulates bone growth and turnover *in vivo*. PLoS One 2009;4:e7930-7943.
70 Manolagas SC: Wnt signaling and osteoporosis. Maturitas 2014;78:233-237.
71 Li H, Wang Z, Fu Q, Zhang J: Plasma miRNA levels correlate with sensitivity to bone mineral density in postmenopausal osteoporosis patients. Biomarkers 2014;19:553-556.
72 Wang Y, Li L, Moore BT, Peng XH, Fang X, Lappe JM, Recker RR, Xiao P: MiR-133a in human circulating monocytes: a potential biomarker associated with postmenopausal osteoporosis. PLoS One 2012;7:e34641- 34651.